UNIVERSITY OF OTTAWA

uOttawa

MASTERS THESIS

Void Fraction in Packed Bed Combustion

Pedro Lovatti Costalonga

Thesis submitted to the University of Ottawa
in partial Fulfillment of the requirements for the

MASTER OF APPLIED SCIENCE (MASc)

in Mechanical Engineering

Department of Mechanical Engineering
Faculty of Engineering
University of Ottawa

Abstract

Packed bed combustors burn fairly large solid fuel particles within confining walls, with air supplied from below the grate. As combustion occurs and particles are consumed, fresh particles are fed onto the bed so the level is kept roughly constant. Packed bed combustion is used for wood and biomass combustion in small-scale power plants, wood waste combustion in pulp and paper plants, and trash incineration. The structure of a packed bed is very important to the combustion process and can be defined by particle shape and size, sphericity, particle overlap (decreasing area availability) and chiefly by void fraction. Void fraction has already been proven of great influence in packed beds – it is raised to the third power in the pressure loss equation, and it can also affect heat and mass transfer and surface reaction rates.

This thesis presents results of several experimental combustion tests that were performed in a packed bed combustor, using commercial spruce lumber particles of parallelepipedal geometry as fuel. At the end of each test the bed contents were removed, taking care to preserve their structure, and fixed with liquefied wax. The solidified bed was then cut into circular cross sections at different heights of the bed, and photographs of the cross sections were taken so the local void fraction could be estimated using image analysis. The bed sampling led to the discovery that, surprisingly, the actual bulk void fraction in the combustor, which is the average of local void fraction measurements, is less than that of the unburnt particles, varying from 19% to 30% in decrease in void fraction depending on the particle type used. Local measurements allowed the development of an empirical linear equation model to represent the variation of void fraction with height above the grate. Each combustion test had measurements of gas volume fractions and temperatures at different heights above the bed grate to be compared with the results of a numerical model simulation.

The numerical model used in this work is an existing numerical model of all the relevant processes in packed bed combustion. Previously, the numerical model had assumed the void fraction to be constant and equal to that of the unburnt fuel, since no information on local variation was available, and the packing geometry remained self-similar as particles are consumed. Three models for void fraction were then compared in the combustion model: a constant void equal to that of the unburnt particles, the empirical linear fit of void fraction with height, and a constant void equal to the measured bulk void fraction. Maximum temperatures were higher using the unburnt fuel void fraction because of a thicker oxidation zone, whereas the void fraction model

based on experiments generated a thicker reduction zone and therefore higher *CO* concentrations. *CO* concentrations were experimentally measured and agreed quite well with the *CO* concentration from the model. Local void fraction differences had the most impact in the diffusion-controlled zone, as shown by comparing the empirical void model and the measured bulk void fraction. How lowering the void fraction can increase gas velocities, heat and mass transfer coefficients, and burning rates is also discussed in this work.

Acknowledgements

I would like to thank my supervisor, Dr. William Hallett, for his time and unwavering assistance towards this work. They were very important, along with his expertise, in formulating the methodology and editing this manuscript. I am beyond honored to have worked with him, and I will be forever grateful.

I would also like to thank my family for their unparalleled love. I am grateful to my wife for being supportive and motivational all along. I am forever indebted to my parents for their valuable counsel and for supporting my decisions.

In addition, I would like to acknowledge and express my sincere gratitude to the Natural Sciences and Engineering Research Council of Canada (NSERC) for the funding provided to this research.

Table of Contents

List of Figures

List of Tables

Table of Nomenclature

Symbol	Name	Unit
A_{CO_2}	pre-exponential factor for CO_2 reduction reaction	kg/m^2 kPa s
a_B	specific surface area of the packed bed	
A_{CO}	pre-exponential factor for oxidation reaction	kg/m^2 kPa s
a_I	particle internal specific surface per unit solid volume	m^2/m^3
a_p	surface area of the particle	m^2
a_v	surface area of a volume-equivalent sphere	m^2
d_i	diameter of the size class i	m
D_{ieff}	effective axial diffusivity	m^2/s
$d_{v,s}$	Sauter mean diameter	m
d_v	volume-equivalent sphere diameter	m
dV_V	void volume	m^3
E_{CO_2}	activation energy for CO_2 reduction reaction	kJ/gmol
E_{CO}	activation energy for oxidation reaction	kJ/gmol
h_s	thermal enthalpy of the solid	J/kg
h_{SG}	heat transfer coefficient	W/m^{2}K
k_{Geff}	effective thermal conductivity of the gas	W/mK
k_{Seff}	effective thermal conductivity of the gas	W/mK
m_P	mass of particle	kg
p_{CO_2}	partial pressure of CO_2	kPa
p_{O_2}	partial pressure of O_2	kPa
r_{CO}	rate of production of CO	kg/m^3 s
T_G	temperature of the gas	K
T_S	temperature of the solid	K
v_G	superficial velocity of the gas phase	m/s
v_p	volume of the volume-equivalent sphere	m^3

v_s	superficial velocity of the solid phase	m/s
X_i	volume fraction of the size class	
Y_i	mass fraction of species *i*	
Y_W	mass fraction of unpyrolyzed wood in fuel particle	
ΔH_{RC}	enthalpy of reaction of the char	J/kg
ΔH_{RCO}	enthalpy of reaction of the CO	J/kg
A	cross-section area	m^2
A_p	pre-exponential for pyrolysis reaction	s^{-1}
dV	container volume	m^3
dx	slice thickness	m
G	carbon conversion rate per unit particle surface area	kg/m^2s
h	relative bed height above the grate	
HPDR	height to particle diameter ratio	
R	universal gas constant	J/kgK
r_i	rate of production of species i,	kg/m^3 s
r_p	rate of pyrolysis reaction	$kg/(m^3s)$
TPDR	tube to particle diameter ratio	

Greek Letters

ε	void fraction	
ε_A	void fraction of a cross-section area	
ε_P	particle porosity	
$\varepsilon_{unburnt}$	void fraction of the packing with unburnt particles	
ρ_{F0}	initial fuel density	kg/m^3
ρ_G	density of the gas phase	kg/m^3
ρ_s	density of the solid phase	kg/m^3
Φ	particle sphericity	
ζ	proportion of particle surface area that is end grain	

η	particle surface availability
τ	tortuosity of particle pore

Chapter One: Introduction

1.1 Introduction

An overfeed packed bed combustor is a combustion system that lets fairly large particles of solid fuel sit and burn on top of a grate, with air being supplied from beneath it, and having surrounding walls to confine the fuel. During this combustion process, different zones will occur inside the overfeed bed: oxidation, reduction, devolatilization, and drying as the distance from the grate increases; only very thin beds lack a reduction zone. Secondary air may be necessary to burn the volatiles in the gas phase above the bed surface. The processes in a packed bed combustor can be seen in Figure 1.1: fuel particles are fed from above and are rapidly dried, and subsequently devolatilized, which will provide char to the combustion reactions closer to the bottom of the bed – reduction and oxidation. At the bottom of the bed char particles are oxidized, but after the oxygen in the air has been completely consumed char reacts with the CO_2 product, which is then reduced to CO. After the particles are completely consumed ash will accumulate on the bed grate.

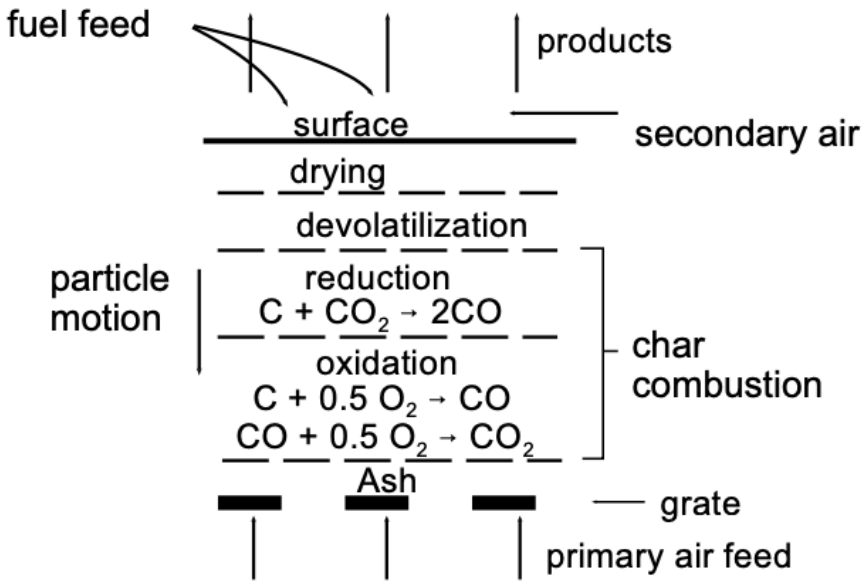

Figure 1.1. Schematic of the reaction zones in an overfeed packed bed combustor.

Specific application examples of packed bed combustion are trash incineration, and wood and biomass combustion in small-scale power plants. Gasification can be deemed to be a related application, given that the essential difference between gasifiers and combustors is the increased thickness of the bed of the former. This in turn will make the reduction zone much thicker (for a specific particle size, the stoichiometry of an overfeed bed is determined mainly by bed thickness). Given the similarities between a gasifier and a packed bed combustor, literature on gasifiers will be included in this work, mainly where the packed bed combustor's literature is scarce.

Just as important as the thickness of the bed to the definition of a packed bed combustor, is the solid fuel type – coal, coke, charcoal, or biomass, and the structure of the bed, where the latter can be defined by particle size and shape, particle overlap, and chiefly void fraction or porosity, a parameter that represents the volume fraction of "void" space in the bed. The void fraction in a packed bed has been extensively studied; the interest in it goes beyond packed bed combustion and many diverse applications can be found in the literature (von Seckendorff & Hinrichsen, 2020). The void fraction is affected by a number of parameters that will be discussed in this work, such as particle and container size, particle shape (mostly defined by the shape factor sphericity), method of packing (intensity and height of particle drop), particle size and shape distribution, and particle material. Other relevant concepts in the local void fraction context are the wall and end effects. Closer to the wall or end of a packed bed, the particles will tend to pack more regularly, causing the void fraction to vary greatly, mainly for more spherical particles.

Most research on void fractions in a packed bed uses spherical, cylindrical, disk-shaped, or elliptical particles, which makes a relationship between particle dimensions and the void fraction more predictable compared to works involving ill-defined or parallelepipedal particles. In the present work, the fuel particles are parallelepipeds of different shapes, and each particle type will form a different packed bed structure.

There are two common methods used to find the bulk void fraction, the one that represents the average void fraction in the whole bed: water displacement and weighing a known packing volume. While the former has several difficulties, such as eliminating air pockets, determining of meniscus level, and the need of wetting the particles in case of porous and dry particles prior to doing the test, the latter can be cumbersome for larger volumes of packing (Dixon, 1988; Girgis & Hallett, 2010). Local void fraction, also known as void fraction area, is the void fraction of a small part of a packed bed, and it can vary in both the axial and radial directions. Most researchers assume

void fraction to be constant throughout a burning bed, but there are a few papers that indicate that it is not. Measurement techniques for the local void fraction can be categorized into destructive and non-destructive. Destructive techniques are based on the pouring of molten wax or curable resin to fill the void space of a packed bed and immobilize the particles, followed by slicing the bed and image analysis of the cross-sections. This makes it impossible to retrieve the bed particles for other analyses. Non-destructive methods include expensive techniques such as gamma and X-ray tomography, and 3-D magnetic resonance as examples, thus making the bed retrievable.

Experimental apparatus for sampling a packed bed combustor or gasifier and therefore having the capability of investigating the void fraction, either local or bulk, after an experimental test is rare but can be found in a few works. The void fraction is known to influence the bed consumption rate, bed reaction rate, solid, and gas temperatures and the thickness of all the reaction zones. Although combustors and gasifiers may have similar reaction zones, the comparison between them needs to be done carefully, as usually gasifier models have insufficient resolution of the oxidation zone.

One influence of the void fraction on packed bed combustion is already known to be strong: it appears raised to the third power in the packed bed pressure loss equation (Trudel & Hallett, 2017). If the void fraction is lowered, the pressure loss is increased substantially. The effect of pressure loss in this work is negligibly small; however, through similar mechanisms void fraction is also known to substantially affect heat and mass transfer processes in the bed by changing the interstitial velocity. Void fraction also directly affects the specific surface area of particulate in the bed: a decrease in void produces an increase in specific surface and hence in the solid reaction rate. Though information on void fraction variation with bed length is only available for gasifiers, the understanding of the void fraction behaviour in a packed bed combustor might be even more important: the oxidation zone is diffusion-controlled and is highly dependent on the interstitial velocity, so it is expected that the void fraction affects this zone more strongly. This zone is relatively thicker in a combustor than it is in a gasifier, so its influence can be assumed to be much stronger.

1.2 Research Objectives

Information on the bulk void fraction after a combustion trial and the variation of the local void fraction in a burning bed are scarce in the literature, as will be shown in the next chapter, and so are their effects on combustion rates. There are a few papers on void variations in gasifiers, but they give conflicting information; furthermore, gasifiers have much deeper beds than combustors, and are not directly comparable. Therefore, the main objective of this work is to measure bulk and local void fractions in an existing combustor bed, and in particular to see if these differ significantly from the void fraction of a bed of unburnt fuel. A secondary objective is to determine through numerical modelling what effects variations in void fraction might have on the processes of combustion in the bed.

The same overfeed "pot" combustor was used in this work as was first used in the work of Ryan and Hallett (2002) and subsequent works (Girgis & Hallett, 2010; Hallett et al., 2013; Trudel et al., 2018). They have assumed that the void fraction is constant throughout the bed, except for the accumulation of ash on the grate, although particle size is allowed to vary. This void fraction was equal to that of unburnt fuel, measured by weighing a known packing volume of particles in a container with the same diameter as the combustor. In this work, the measurement of the bed void will be done by filling the bed with wax, cutting the solidified bed into transversal planes and using image analysis to analyse the cross-sections of the slices.

Several packed bed combustion experiments were run using wood fuel cut into parallelepipedal shapes, the resulting beds were sampled and the void fractions at several different positions were found. From this, an empirical model of void fraction axial profile can be generated, or, alternatively, the mean void fraction can be calculated and used as the bulk void fraction. An existing 1-D finite volume method model that contains the most relevant processes of packed bed combustion of char was used, so a comparison of the combustion model outputs with three different void fraction models can be done: the void fraction of unburnt fuel, the void fraction averaged from image analysis readings and the empirical model for the void fraction.

Chapter Two: Background and Literature Review

2.1 Introduction

This chapter provides a brief overview of the background on the void fraction in packed beds, such as important parameters that can affect it, and the measurement methods, the existing types of fuel bed combustors, the structure of an overfeed packed bed combustor, and the known effects of the void fraction on packed bed combustion.

2.2 Void Fraction in Packed Beds

The understanding of void fraction in a particle bed is of great importance for many different fields. Examples include the ceramic industry (with the probable exception of glasses and glaze materials), catalytic reactors, absorbers, heat exchangers, distillation columns, immobilization of bacteria and enzymes in pellets or beads, chromatography columns, civil engineering, packed bed solar energy storage systems, packed bed gasifiers and packed bed combustors, to name but a few (Benyahia, 1996; Cooke & Rowe, 1999; Dorn et al., 2017; Hobbs et al., 1992; Singh et al., 2010; Trudel et al., 2018; Westman & Hugill, 1930).

A packed bed consists of solid particles with gas (or liquid) filling the interstices or "voids" between them. The void fraction is defined as the fraction of the entire bed volume that is composed of these "voids". Therefore, the higher the void fraction of a certain packed bed, the more gas volume this bed will have, and consequently less solid volume. For a packed bed reactor, the importance of these voids will be mainly to allow the air or other gases to flow through them. It is also important to note that if a cross-section is taken of a packed bed, the void volume fraction will be equal to the fraction of void area seen in the cross-section. If the void fraction of a cross-sectional area A is ε_A, then the volume of void in a slice of thickness dx is given by eq. (2.1), which by definition gives the void fraction ε of the total volume V.

This definition is important because it permits the estimation of a packed bed void fraction by averaging fractions of void areas or local void fractions.

$$dV_V = \varepsilon_A A\, dx = \varepsilon\, dV \quad \textbf{(2.1)}$$

As a cylindrical-shaped container is the most common in the literature, the most applied in industry, and the subject of this study (a "pot" combustor), it will be therefore the one analyzed and discussed here. Packed bed containers of uncommon shapes, such as rectangular (Beavers et al., 1973; Taguchi et al., 2006), annular (Caulkin et al., 2009), non-rigid balloon-shaped (Bernal & Finney, 1967; Susskind, 1966) and spherical (Man et al., 2005) can also be found in the literature. Other examples of influencing parameters on the void fraction are the particle shape, the particle material, the boundary effects, such as wall and end effects, and the ratio of container size to particle size, the particle shape and size distribution in the bed, the container inside wall shape, and how the particles are deposited in the bed. The last includes two factors: the applied intensity of deposition, representing the number of particles falling into the bed at the same time, and the height of drop, which affects the velocity of particles arriving in the bed.

2.2.1 Important Parameters in the Definition of Void Fraction

2.2.1.1 Particle Shape

Particles of numerous different shapes have been used in the literature: spheres (Benenati & Brosilow, 1962; Farrell et al., 2010), cylinders (Dixon, 1988; Zou & Yu, 1996), Raschig rings (Gan et al., 2004; Roblee et al., 1958), trilobes (Farsi et al., 2021; Nguyen et al., 2005), ellipsoids (Gan et al., 2016; Romanova et al., 2020), cubes (Lufeng Liu et al., 2017), polyhedrons (Jia et al., 2007), parallelepipeds (Montillet & Le Coq, 2001; Trudel & Hallett, 2017), disks (Berryman, 1983; Desmond & Weeks, 2009), prisms (Zou & Yu, 1996), Berl saddles (Roblee et al., 1958) and wood chips (Hamel & Krumm, 2008; Lee & Bennington, 2005).

The particle diameter d_v is the diameter of a volume-equivalent sphere v_p and is given by eq. (2.2), in the case of non-spherical particles, while for spheres, d_v will be simply the diameter of the sphere. It is also important to note the definition of the Sauter mean diameter, an average particle size for the case of a packed bed composed of non-uniformly sized particles. It is given by eq. (2.3), where N is the number of particle size classes, X_i is the volume fraction of the size class

i in the solid phase, and d_i the diameter of the size class i. The Sauter mean preserves both the total solid volume and total particle surface area of the bed.

$$d_v = \left(\frac{6v_p}{\pi}\right)^{1/3} \tag{2.2}$$

$$d_{v,s} = \frac{1}{\sum_{i=1}^{N}\left(X_i/d_i\right)} \tag{2.3}$$

The particle shape is frequently related to the particle sphericity Φ, given by eq. (2.4), where a_v is the surface area of a volume-equivalent sphere, and a_p is the actual surface area of the particle. It represents how spherical a particle is, therefore the sphericity will be equal to 1 for a sphere, and less than 1 for non-spherical particles. Although the most frequently used shape parameter, the sphericity does not uniquely define a shape – it is possible for particles to have quite different shapes with the same sphericity.

$$\Phi = \frac{a_v}{a_p} \tag{2.4}$$

The effect of the lower sphericity of the particles on the bulk void fraction of a packed bed is to increase the latter. Haughey & Beveridge (1969) attribute this to "bridging", the formation of an arch structure in the bed, as any angularity in shape may help such a structure to develop. However, Yu & Standish (1993) and Zou & Yu (1996) showed that this is not always true, as for dense random packings the void fraction can decrease with higher sphericities of a certain range. They have demonstrated that sphericity alone is not capable of predicting void fraction, given that disks and cylinders with similar sphericities have a big disparity in void fraction and particles with other shapes should have values of void fraction between those two.

The specific surface area is an important parameter for some packed beds, such as reactors, and represents the area of a particle surface per unit of bed volume. The specific surface area is dependent on the variables mentioned here: the void fraction ε, the particle diameter d_v, and the sphericity φ, and is given by eq. (2.5), where η is the particle surface availability, given by the particle surface area in contact with flow divided by total particle surface area. A decrease in the void fraction is, therefore, equivalent, to an increase in bed depth or a smaller feed particle because they would result in a larger specific surface area (Cooper & Hallett, 2000; Trudel et al., 2018).

$$a_B = \frac{6(1-\varepsilon)}{(\varphi d_v)} \quad \textbf{(2.5)}$$

2.2.1.2 Particle Material

A great variety of particle materials have been used in the literature regarding packing and void fraction: lead (Benyahia, 1996; Westman & Hugill, 1930), glass (Comiti & Renaud, 1989; Zou & Yu, 1996), ceramic (Cooper & Eaton, 1962), steel (McGeary, 1961; Raichura, 2010; Westman & Hugill, 1930), stone (Debbas & Rumpf, 1966), sand (Ozawa et al., 1996; Westman & Hugill, 1930), plastic (Nolan & Kavanagh, 1995; Zou & Yu, 1996), metal (McGeary, 1961), edibles (Westman & Hugill, 1930; Zou & Yu, 1996), coal (Krishnudu et al., 1989), ash (Ryan & Hallett, 2002), and wood (Hamel & Krumm, 2012; Porteiro et al., 2010; Zou & Yu, 1996).

On the other hand, studies on the particle material's effect on the void fraction are scarce and point towards different directions. Koekemoer & Luckos (2015) compared three different materials: ash, coal, and char, all of which had the same Sauter mean diameter, and found the ash to have the highest void fraction followed by char and coal. This was attributed to both lower sphericity and higher surface roughness, a trend that was agreed upon by Crawford & Plumb (1986), who tested smooth spheres and spheres with roughness elements added to the surface, and Pottbäcker & Hinrichsen (2017), whose work was based on the comparison of spheres of polyamide, polyoxymethylene, aluminum, glass and steels with different roughness.

In disagreement with these studies are Macrae & Gray (1961), who found a slight difference in void fraction due to a change in surface roughness, although the Pottbäcker & Hinrichsen (2017) and the Macrae & Gray (1961) papers agreed on the fact that a higher coefficient of restitution (e_{ss}), which is the measure of elasticity of the collision between particles, helps to improve the packing of particles, thus decreasing the void fraction. Another study showed by comparing previous works, and their own tungsten and steel shot packing experiment, that particle materials do not much affect the resulting porosity (McGeary, 1961). Finally, a completely opposite result states that smoother materials have a slightly higher overall void fraction (Schuster & Vortmeyer, 1980), based on a comparison of lead shot and glass balls, and radial void fraction profiles were significantly different.

Container wall material effects are not discussed in the literature, but the study of internal wall structure effects on the packing of particles can be found. Niu et al. (1996) used a lining sheet

of regularly arranged, convex hemispheres at the walls of a bed of spheres and found it to decrease the wall effect by reducing the sharp rise in void fraction near the wall, and a more uniform profile of radial void fraction was exhibited. Zobel et al. (2012) used a hexagonal array of hemispheres that reduced the peaks and valleys of the void fraction distribution by just a little compared with the case of the plain wall, although a wave-like wall structure resulted in a much more homogeneous void fraction profile.

2.2.1.3 Particle Size and Shape Distribution

It is well known that increasing the width of the particle size distribution reduces the void fraction, as smaller particles fill the interstices between larger ones (Hoffmann & Finkers, 1995). The packing of a binary mixture of spheres was first analyzed by Westman & Hugill (1930). In their work, coarse and fine, medium and fine, and medium and coarse binary mixtures of sand were evaluated and they concluded that the packing of the bed becomes optimum (i.e., the void fraction is minimum) when 30% of the mixture's composition is made of the smaller size particles. Binary mixtures of large and small particles with 50% volume composition each were packed into containers of different diameters, and it was found that increasing the large-to-small particle diameter ratios effectively reduces the bed void fraction (Foumeny et al., 1991). Lastly, Sohn & Moreland (1968) compared the effects of changing both the size ratio of binary mixture particles and the composition of the larger component of a binary mixture on the void fraction, and it was observed that the volume fraction of the large component for optimum packing decreased to roughly 50% for smaller size ratios, from 70% for larger size ratios.

Multi-sized particles of sand of mean sphericities 0.81 and 0.86 were experimentally investigated and a proportional relationship between packing density and the dimensionless standard deviation of the particle size distribution was established, except for the region between 0 and 0.1 of the dimensionless standard deviation for the less spherical particles. The rate of change in the packing density with increasing dimensionless standard deviation was different for the particles with different sphericities: the less spherical particles had a more rapid decrease in the void fraction compared to the more spherical particles since the more spherical particles lost their advantageous packing character as the size distribution width increased (Sohn & Moreland, 1968).

The packing of a mixture of particles with different shapes was investigated by Hallett et al. (2019) and Yu et al. (1993). In the former, the void fraction of packing of a mixture of

parallelepipedal particles of about the same size and different shapes was studied. Packing of a mixture of particles with very different shapes presented a void fraction almost as high as the void fraction of the bed of a pure component and looser packing, because the filling of each other's interstices was prevented by their shapes. However, another mixture of particles with roughly the same difference in sphericity, compared to the previous mixture, had an intermediate value of void fraction - between those of the packings of single components of this mixture - due to one of particles having a nearly cubical shape. Three different mixtures are presented in the work of Yu et al. (1993), with a larger cube separately mixed with the following: a smaller cube, a smaller sphere, and a larger sphere; and their minimum void fractions were respectively reached at the following volume fractions of the larger cube: 50%, 50% and 70%, where the mixture with the smaller sphere had the lowest minimum void fraction, given the capability of the smaller spheres to fill the large cube's interstices. Also, in the latter the work of Milewski (1973) is cited and plotted, in which mixtures of fibers of different length to diameter ratios and spheres were investigated, where the diameter ratio of the spheres to the fibers was kept at 17.4. The volume fraction of spheres for an optimum packing increased with the length to diameter ratio of the fiber from roughly 0.7 for a length to diameter ratio of 3.91 up to 1 for a length to diameter ratio of 37.12.

2.2.1.4 Boundary Effects

Boundary effects involve two of the most important factors for the packing of particles, the tube-to-particle-diameter ratio and the height-to-particle diameter ratio, which have the wall and end effects as determinant factors to their definitions.

One elementary point in the structure of the packed beds is the wall and end effects. The particles heaped in a container will naturally settle and align with the container's walls (von Seckendorff & Hinrichsen, 2020); this will cause the void fraction to be larger at the wall, because the solid wall prevents the particles from packing as closely as they do otherwise, and the void fraction may oscillate in the radial direction up to a point where the wall effect is no longer present. The end effect is analogous to the wall's, although the wall, in this case, is the surface of the container that supports the particles, the bottom of the bed, and the axial void fraction profile is oscillatory (Benyahia, 1996). To avoid these effects as much as one can, the tube-to-particle

diameter ratio and height-to-particle diameter ratio need to be maximized, although the extent of these effects is also dependent on the particle shape (Benyahia & O'Neill, 2007).

The tube-to-particle diameter ratio (TPDR) is the relation between the packed bed container diameter and the particle diameter. Several works on the analysis of the effect of the TPDR on both the bulk void fraction and radial void fraction profile are available. The TPDR is also important when accounting for wall effects in measuring the bulk void fraction, as the effect of the wall only extends a certain number of particle diameters from the wall, and that in turn can be investigated by the radial void fraction distribution.

It is intuitive to assume that a larger TPDR will generate lower bulk void fractions given that with increasing TPDR the size of the wall effect layer becomes relatively smaller compared to the tube diameter, thus decreasing the bulk void fraction. This assumption is right for the majority of applications of packed beds, except those of extremely low TPDR. Dixon (1988) experimentally evaluated the relationship between TPDR and bulk void fraction for spheres and cylinders, and up to a point, an increase in the former caused the bulk void fraction to increase as well, followed by a successive decrease. That trend was also seen in the works of Benyahia & O'Neill (2007), Foumeny et al. (1991), Klerk (2003), and Zou & Yu (1995). For the packing of spheres, the bulk void fraction approaches a constant value for a TPDR equal to or higher than 10, as one can see in the literature review of von Seckendorff & Hinrichsen (2020) and in the work of (Foumeny et al., 1991). This value is expected to be lower for non-spherical particles, since the extent of the wall effect is lower compared to that of spheres, given the higher randomness of packing (Benyahia & O'Neill, 2007; Hamel & Krumm, 2008, 2012).

The radial void fraction distribution is very important when addressing the wall effect in a packed bed. It also shows some general behaviour for a packed bed, mainly seen for spheres, such as that the minimum local void fraction is located at around half a particle diameter from the wall, and that the void then rises to another maximum, excluding the wall location, at approximately one particle diameter from the wall (Klerk, 2003). Although mainly seen in packings of spheres, an oscillatory void fraction radial profile was also observed in this work using an example from Küfner & Hofmann (1990) that investigated packings of cylindrical particles. This situation was addressed also by (Benyahia, 1996) who investigated several cylinders with different aspect ratios to find that the first maximum and minimum depend on these aspect ratios.

The wall and end effect extent of penetration is deemed to vary with TPDR and between shapes as well. For irregular particles such as wood chips, the importance of the wall effect decreased (Hamel & Krumm, 2008). A decrease in sphericity will cause the wall and end effects to vanish more rapidly, evidence suggests (Montillet & Le Coq, 2001; Roblee et al., 1958). This can be explained by the tendency of the packing of non-spherical particles to be more irregular than spherical particles packings, so the bed wall and end would not affect them as much. For spherical and equilateral cylindrical particles the general trend was an increase in the extent of the wall effect for larger a TPDR, while for non-equilateral cylinder no trend could be identified (Benyahia, 1996).

The height-to-particle diameter ratio (HPDR) is the ratio of the packed bed container height to the particle diameter, and analogously to the TPDR, the HPDR will influence the bulk void fraction and the axial extent of the end effect. Zou & Yu (1995) studied the effects of changing the HPDR on the bulk void fraction in a packed bed of spheres and their results show that they are inversely proportional and that different HPDR values do not seem to affect the curve shapes of void fraction versus TPDR. An increase in HPDR caused the wall effect distance to increase for spherical particles, whereas cylindrical particles, either equilateral or non-equilateral, are not much affected (Benyahia, 1996).

2.2.1.5 Intensity of Deposition and Height of Drop

The intensity of deposition refers to the number of particles that fall onto the packed bed top opening per unit of time. An improvement in packing, and consequently a decrease in void fraction, can be noticed when a lower intensity of deposition takes place. The reasoning for this is that the particles have more time to settle in the bed and not be disturbed by neighbouring particles, whereas higher deposition intensity makes particles interact with one another more frequently, ultimately hindering their settling in the bed.

Afandizadeh & Foumeny (2001) used spheres to study three different intensities of deposition, which were called fast, slow, and “snow storm” filling and the trend was the same for packed beds with five different particle diameters. Zhang et al. (2021) evaluated the same effects using cylinders of different aspect ratio and all of them resulted in a lower void fraction for a lower intensity of deposition. This work also showed that the critical filling rate (the point at which an

increase in intensity deposition does not affect the void fraction much) decreases with an increase in aspect ratios.

Finally, Macrae & Gray (1961) investigated the effect of deposition intensity on spheres of five different packing materials: lead shot, glass, polystyrene, steel, and phosphor bronze. Although steel and glass had the anomaly of improving in packing as the intensity of deposition increased up to a certain value, the ultimate trend pointed towards a decrease. This research also brought the influence of the height of drop on the improvement of packing, as it was found that the higher the height of particle drop gets, the better particles in the bed appear to pack, thus decreasing void fraction, and this effect is best noticed for lower intensity deposition rates. These effects were both confirmed in cylindrical particles by Tangri et al. (2017).

2.2.2 Void Fraction Measurement Techniques

A classic approach to finding the bulk void fraction of a packed bed is to weigh and pour particles into a container (cylinder), and when the bed gets to the desired level, the height of the packed bed is measured. Since the cylinder volume is dependent on the height and base area, which is known, the volume can be calculated, as well as the volume of particles poured in, since the particles' weights are measured and their densities are previously known. Hence, by calculating both the cylinder and particles' total volume, one can find the bulk void fraction (Dixon, 1988; Westman & Hugill, 1930; Yu et al., 1992).

Another classic approach is to calculate the void fraction by water displacement. A known amount of water is poured into a packed bed container, the water fills the voids, and the void fraction is found from the final volume of water added and the volume of the container (Benyahia & O'Neill, 2007; Foumeny et al., 1991; Girgis & Hallett, 2010). Although this is one of the most common techniques, it may present some difficulties: elimination of air pockets, determination of the proper meniscus level, and the need to soak porous particles before the measurements.

Local void fraction measurement techniques have been separated into two categories by Hamel & Krumm (2012). The first category includes destructive techniques, which are based on the solidification of the whole bed and incremental removal. Molten wax or curable resins are poured into the packed bed, and after its solidification, the bed is machined or cut into axial slices. These slices' faces are either investigated with image analysis to assess the void fraction (Benyahia,

1996; Hamel & Krumm, 2012) or the slice's filler material is removed and weighed so the weight difference is assessed (Benenati & Brosilow, 1962; Goodling et al., 1983; Roblee et al., 1958). The centrifuged packed bed is another technique used to assess the local void fraction as a function of radial position. In this technique, a liquid, normally water, is incrementally added to the packed bed and the drum is rotated so as to generate an annular layer of a certain constant height and variable thickness. Water is added until the annular liquid ring thickness is increased to the point that it gets close to the axis of the rotating drum (Ridgway & Tarbuck, 1966).

Non-destructive techniques include X-ray tomography of the whole packed bed (Auwerda et al., 2010), in which images of several slices in the bed are obtained, and image analysis is then performed at different bed levels. Magnetic resonance imaging can be performed in a similar fashion to investigate local structures of a packed bed (Sharma et al., 2001). Glass spheres filled with coloured liquid or coloured glass particles have been used to fill a transparent glass vessel set up on a Plexiglas plate, which is illuminated from below so that the particles can be visualised (Schneider & Rippin, 1988). Individual particle measurement is another non-destructive technique alternative. This involves introducing the particles into a transparent container that has outside walls scribed with a measuring grid, after which the particles between successive grid lines are counted and the particle distribution is quantified (Pillai, 1977).

Finally, in order to find the bulk void fraction derived from image analysis of radial cross-sections at different heights, which is the technique used in this work, one should simply average these local void fractions. To check the accuracy of the image analysis measurements used to find the bulk void fraction of a packed bed, comparisons between bulk void fractions from gravimetric measurements and image analysis averages are available in the literature, and they agree well. A difference in the void fraction in a packed bed of wood pellets of 3.94, 1.24, and 1.25% was found in the work of Hamel & Krumm (2012) and from 1.56 to 4.83% in a packed bed of wood chips (Hamel & Krumm, 2008) against 2 to 5% according to Montillet & Coq (2003).

2.3 Types of Fuel Bed Combustion

Among applied technologies for biomass combustion, fuel bed combustion is one of the most widely accepted and used due to its lack of sensitivity to the fuel composition, moisture, particle size, and impurities, and the fact that it requires a minimum of fuel preparation. There are three

types of fuel bed combustor settings and they all have air supplied from below the grate blowing upwards, as Figure 2.1-Figure 2.3 show. They can be distinguished as to whether the fuel and air are in counterflow, crossflow, or cocurrent flow (Hallett, 2009).

Counterflow, also called overfeed combustion is a process that has fuel particles evenly distributed over the bed, and as this fuel burns and is consumed, fresh fuel is dumped onto the burning bed and moves downwards towards the grate in the opposite direction to the airflow. Ash remaining is dumped through the spaces between the bed grate bars.

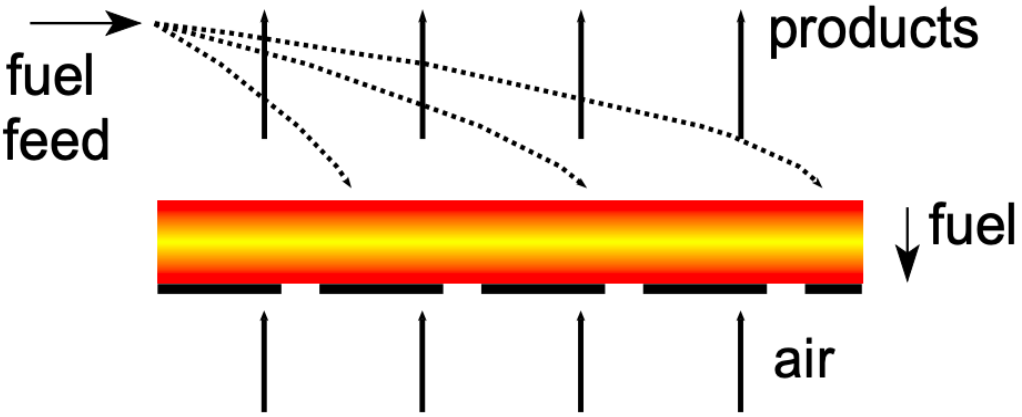

Figure 2.1. Overfeed Bed Combustion Setting

In a crossflow combustion setting the fuel and air motion need to be perpendicular to each other. The fuel can be supported by a traveling grate on one end of which the fuel is fed, and at the other end the ash remaining is dumped. Different airflow rates are assigned for different zones of this grate since air requirements and combustion rates can vary considerably at different sections of the bed. The inclined grate is an alternative mode of crossflow combustion: in this, the fuel slides down as it burns, often with the help of cylinders to push the fuel down the grate at different steps.

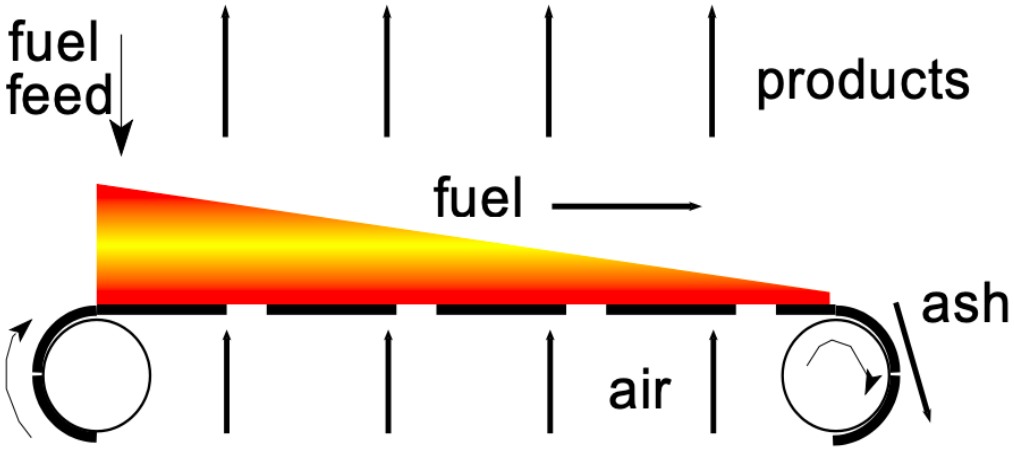

Figure 2.2. Crossflow Bed Combustion Setting

In a cocurrent flow setting, also known as underfeed combustion, the fuel feed is pushed up from below the grate, though in practice this type of process can never exist by itself, as fuel is supported and moved sideways as well with the support of grates, hence a mixture of cocurrent flow and crossflow occurs.

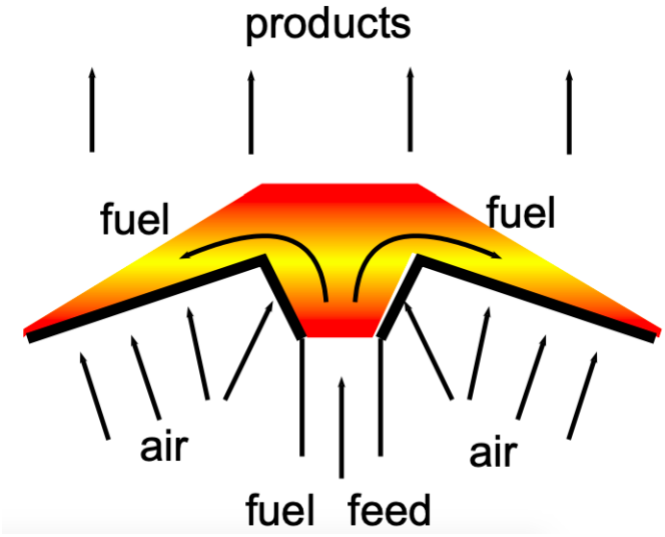

Figure 2.3. Underfeed Bed Combustion Setting

2.4 Structure of an Overfeed Bed Combustor

The present work concerns itself only with overfeed combustion, the most common object of tests and models, and the simplest fuel bed configuration; therefore, more details will be given for this mode of combustion. An overfeed packed bed combustor can be separated into four main different

reaction zones: oxidation, reduction, pyrolysis, and drying as height above bed grate increases. Figure 1.1 shows these zones in the bed. The oxidation zone is the hottest region in the combustor, as oxidation occurs on the surface of the char, generating initially CO and thereafter CO_2, due to the oxidation of CO. The reduction zone, where the CO_2 will react with the char in the bed and form CO, is endothermic, and therefore colder than the oxidation zone. The pyrolysis zone occurs in the second topmost layer of the bed, and its main function is to supply char to the oxidation and reduction zones, as volatiles are expelled from the wood. Drying will take place in the topmost region of the bed, where all the moisture from the fuel is evaporated, and it will occupy the smallest zone in the bed as it will occur quickly (Cooper & Hallett, 2000; Hallett, 2009).

The oxidation and reduction zone will comprise most of the bed volume. Usually the reduction zone is thicker than the oxidation zone, since the oxidation zone is very thin, typically one particle diameter thick. This bed thickness is maintained constant throughout the whole combustion process by feeding fresh fuel on top of the bed to make up for the shrinking char. As briefly mentioned in Chapter 1, the thickness of the bed will largely define the stoichiometry of a packed bed combustor. For a bed with a specific particle size, the thicker the bed, the more CO will be produced, and increasing the airflow rate will only affect the char consumption, and not the stoichiometry.

As discussed above, the thickness of the bed is very important in defining an overfeed packed bed combustor. If the bed is sufficiently thick (more than 1 – 2 particle diameters), all the oxygen is consumed in the oxidation layer, and in the next layer, reduction, char reacts with product CO_2 and produces CO. If the bed is very thin (typically one particle diameter in thickness), the oxygen will not be completely consumed in the bed, thus no reduction zone will be formed, so volatiles combustion can start in the bed and end in the freeboard with no need of additional air supply. However, if the bed is thick, all the oxygen is consumed and significant production of CO is observed, since there is a large reduction zone and the CO_2 will have time to react with the char. Due to the endothermic nature of the reduction zone, the bed temperature in the reduction and pyrolysis zones will be lower, and in this case the products will be volatiles and a large quantity of CO. Secondary air (overfire air) will be required to oxidize all this CO in the freeboard, so part of the heat release will occur above of the bed. In order to properly oxidize the CO produced by a thick bed, more furnace volume will be required as well as higher temperatures; this is one of the reasons why operating with a thin bed is desirable. Another one is that if the bed becomes very

thick, the gas compositions at the exit approach equilibrium asymptotically, and this is where gasifiers normally operate.

The essential difference between a packed bed combustor and a gasifier is the thickness of the packed bed: gasifiers have a much thicker bed which is almost entirely composed of a reduction zone. Therefore, some examples in this work will make use of gasifiers as well.

2.5 Known Effects of Void Fraction in Packed Beds

The importance of the study of void fraction in a packed bed is primarily related to the pressure loss: the void fraction is raised to the third power in the pressure loss equation, reflecting the fact that by lowering the void fraction an increased restriction to the flow through the packed bed will be imposed, thus increasing frictional losses (Ergun & Orning, 1949). For packed bed combustion, though, since the bed is shallow, the pressure loss is very small; therefore, it will be neglected in this work.

In packed bed combustors the effect of lowering the void fraction will be to increase interstitial velocities of the gas, and this increases heat and mass transfer coefficients, which will affect the burning rate, efficiency, and emissions. The heat transfer from the gas phase to the solid is also increased due to higher specific bed surface area, which can reduce the gas temperature (Duffy & Eaton, 2013). The above-mentioned effects of lowering the void fraction will ultimately increase the maximum solid temperature as well as decrease the air/fuel stoichiometry as the specific surface area of the bed increases (Cooper & Hallett, 2000).

Furthermore, if the bed void fraction varies radially, another important effect can appear: channelling, a phenomenon caused by a higher local value of void fraction that will reduce resistance to flow, increasing the airflow rate locally. The resulting higher local combustion rate tends to enlarge this channel because particles will be consumed at higher rates locally. Important consequences of the channelling are the production of a high CO and unburnt hydrocarbons in the flue gas and high carbon content in the ash (Duffy & Eaton, 2013; Yang et al., 2003).

2.6 Void fraction in Packed Bed Combustors/Gasifiers

Few works provide experimental apparatus capable of sampling the packed bed after a combustion or gasification test (Conradie et al., 2015; Krishnudu et al., 1989; Bunt & Waanders, 2008; Ryan & Hallett, 2002). Among these, only the latter investigated packed bed combustors, while the other works were on gasifiers. Conradie et al. (2015) presented a laboratory scale fixed bed coal reactor that pivots around a central point to allow the reactor to be rotated and placed in a horizontal position after an experiment; this allowed the inner pipe of the reactor that contained coal, char and ash to be removed without disrupting the bed. The gasifier used by Krishnudu et al. (1989) presented a device for their Lurgi gasifier that allowed the ash to be withdrawn by rotating the grate, and this allowed sequential layers corresponding to 25 cm thickness along the gasifier height (equivalent to 0.25 m^3) to be removed. As the sampling was done, material would have been moved down; however, since the grate was roughly conical in shape, and since some mixing must have occurred during sampling, this is unlikely to have preserved the bed structure. Bunt & Waanders (2008) presented a sampling procedure very similar to Krishnudu et al. (1989), where the ash grate speed of the reactor was controlled at minimum revolutions per hour while discharging the reactor contents. Finally, Ryan & Hallett (2002), allowed the bed to be divided into slices for sampling by lowering the bed in measured increments and cutting it by means of a horizontal transversing slide.

The variation of some of the void fraction influencing parameters, such as particle size, sphericity, and particle size distribution, along the bed length has been experimentally investigated. A decrease in particle mean size with a decrease in height above bed grate was observed in gasifiers (Conradie et al., 2016; Krishnudu et al., 1989; Bunt, 2006), and combustors (Girgis & Hallett, 2010), although the smallest sizes were located in a higher position in the work of (Bunt, 2006) where reduction of size was attributed also to thermal and mechanical fragmentation, and not only to particle conversion.

The particle size distribution width was found to increase as one moves closer to the grate according to the work of Conradie et al. (2016), although quite opposite and different results have also been found. A much earlier Krishnudu et al. (1989) study found that the particle size distribution to become more homogeneous as particles were consumed, and a roughly constant trend was observed in Bunt (2006), although from the drying to the end of the pyrolysis zone an increase of the particle size distribution width is found followed by a decrease of it from the beginning of the gasification zone to the zone immediately above the bed grate. Moreover,

sphericity was calculated from an empirical correlation for pressure drop in a gasifier of pellets (Gunarathne et al., 2014), and it was found to increase as height above the grate decreased, up to a point where an ash bed is formed, in which region sphericity decreased considerably. On the other hand, the sphericity variation of parallelepipedal particles along the bed length in a packed bed combustor has been measured by Trudel et al. (2018) with a vernier caliper and no significant variation could be found.

The local void fraction at different heights above the gasifier grate was measured in several works (Bunt & Waanders, 2008; Conradie et al., 2016; Krishnudu et al., 1989; Mangena et al., 2013).All of them used true and bulk density to calculate the void fraction in each section of the bed, while Gunarathne et al. (2014) calculated local void fractions at different heights of the bed using a pressure drop correlation

Krishnudu et al. (1989) measured the void fraction variation along the length of a 1.13 m of diameter by 3.5 m height gasifier for two different types of Indian coals of an average size of 10.54 mm and 11.56. An increase in void fraction from 0.35 to 0.55 and from 0.47 to 0.7 from top to bottom respectively was found, although the number of particles of less than 6 mm in size increased from 23 to 58% and from 26% to 53%. For most of the distance from the grate up the void fraction is nearly constant, and only varies significantly near the top.

A commercial gasifier was used in the works of both Bunt & Waanders (2008) and Mangena et al. (2013). It was 9 m in height and 4 m in diameter, although the fuel types used differed from each other, the latter utilizing North Dakota lignite and the former South African bituminous coal. Void fraction was not measured directly in either of these works; however, true and bulk density were measured at different bed levels, and therefore void fraction could be inferred. For the bituminous coal, the void fraction varied from 0.3 at the top to 0.6 at the bottom, and a damped oscillation trend of Sauter mean diameter was found from the top to the bottom of the bed, varying from 10 to 6 mm. A local void fraction of 0.4 was found roughly constant with the bed length for the lignite coal; this had a massive decrease in mean diameter at the drying zone, after which diameter stayed approximately constant from the devolatilization zone to closer to the bed grate, varying from 12 to 2 mm.

South African coals were also the type of fuel fed to a laboratory-scale gasifier of 1.2 m in height and 1 m in diameter (Conradie et al., 2016). Unburnt particles of three different mean diameters, 8, 6, and 4 mm were used, and generated void fractions of 0.484, 0.432, and 0.432. After

gasification, the bed presented a void variation from 0.65 at the bottom to a minimum of 0.5 close to the top, and then to 0.55 on the top of the bed for the 8 mm particle. The 4 mm particle had a maximum void fraction on the bottom of the bed of 0.75 and a minimum of 0.45 close to the top, while at the top, the void fraction was 0.55.

Gunarathne et al. (2014) calculated the void fraction based on a correlation from literature between the sphericity and void for cylindrical particles, which causes the procedure to be dubious, as sphericity does not uniquely determine particle shape. A reduction of 6% in the bulk void fraction from fresh to burnt pellets in a gasifier was shown. Regarding the local void fraction, there was a consistent decrease in it from the top layer, which had a void fraction of around 0.5 to the second lowest layer of the bed, that presented a void fraction of 0.404; then the void fraction increased again in the ash layer and had the maximum value of the whole bed overt two runs, 0.54. The reduction in void fraction with decrease in distance from the bed grate is explained by the idea that smaller particles tend to pack more tightly, although this is not necessarily true. Pressure loss parameters are shown to change as conversion proceeds, but no discussion on the effect on conversion is given. Luckos & Bunt (2011) were also able to calculate the void fraction at different zones in the bed (drying, de-volatilization, gasification, and combustion, as the distance from the grate decreased), and their respective void fractions were 0.54, 0.59, 0.49, and 0.30. The bed bulk void fraction range after a gasification run ranged from 0.41 to 0.46 against a previous void fraction range of unburnt particles from 0.436 to 0.522.

The findings of Krishnudu et al. (1989) were further adopted in the model of Hobbs et al. (1992), which assumed a linear variation of void fraction from a minimum value at the bed top to a maximum on the bottom. Hobbs et al. (1992) do not explicitly discuss the void fraction changing heat and mass transfer coefficients, but as they used it to calculate the pressure loss, one would suppose that it does also for the coefficients. This work also displays the effect of varying void – higher void fractions give lower conversion rates, as expected. The model of Chen & Gunkel (1987), on the other hand, assumes that void fraction decreases as particles shrink, and has a simple equation for this relationship, which appears to be based on data for void as function of the ratio between particle diameter and gasifier diameter taken from literature. The model of gasifier used in their work tracks particles through the bed, the bed has 4.5 m of height and particles are poplar of 2 cm.

Duffy & Eaton (2013) proposed a two dimensional solution for a transient combustor with random radial variation of void fraction and constant void fraction in axial direction. The radial variation was described by normal distribution, and local area of larger void is set as the start of the channeling.

Although the literature review provides sufficient data to show that the local void fraction in gasifiers varies within the bed length, no work dealing with its variation in a packed bed combustor was found. The assumption of a constant void fraction along the bed length is used in most works on packed bed reactors and is the standard assumption for modelling, only affected by the ash build up in the bottom of the bed (Bauer et al., 2010; Mehrabian et al., 2014; Porteiro et al., 2010; Ryan & Hallett, 2002; Ryu et al., 2006; Thunman & Leckner, 2005; Van Der Lans et al., 2000; Yang et al., 2005). This may be supported by the idea that since the bed particle geometries remain self-similar along the bed length, then so should the packing geometry (Trudel et al., 2018).

2.7 Conclusions from Literature Review

A review of characteristic quantities in packed beds shows that the void fraction is directly related to the bed specific surface area, and therefore it also affects solid reaction rates. Moreover, the void fraction affects local flow velocities, and consequently heat and mass transfer coefficients, which ultimately should affect combustion rates. There are only a few works in the literature on void variations in packed beds, and these are all for gasifiers, which are not directly comparable to combustors since the bed thickness is so much greater in a gasifier. Until now, the effects of void fraction on combustion have not been explored. The gasifier papers show some variation of void in the reacting bed, and indicate that these variations have some effect on reaction rates, but the conclusions of these papers contradict each other, with some indicating an increase and some a decrease in void with height in the bed. The purpose of this work is therefore to determine experimentally if void fraction varies in a burning packed bed, and if so, what the effect of this variation is on combustion.

Chapter Three: Experimental Equipment and Methods

3.1 Introduction

The goal of this chapter is to provide information regarding experimental tests and methods used in this work in order to find the void fraction of burnt particles in a packed bed combustor, which will be used as input parameters of a numerical combustion model. In addition to the methods used to find the local void fractions, extra information was also gained in the form of proximate analyses at different heights.

3.2 Experiments

3.2.1 Combustor and Instrumentation

Experiments were performed in a laboratory-scale "pot" combustor, used in previous works (Hallett et al., 2013; Ryan & Hallett, 2002; Trudel et al., 2018). The combustor has an inside diameter of 23 cm, and the fuel particles are supported by a stainless-steel grate at the bottom through which the primary air is introduced through a flow straightener and plenum chamber, as shown in Figure 3.1. An afterburner is located above the bed, in which secondary air jets are introduced to burn off the CO and volatiles produced in the bed. Local gas concentrations are measured in the bed at different heights above grate with a water-cooled sampling probe and a gas chromatograph with a 60/80 Carboxen 1000 column, while temperatures are measured with type B wire thermocouples supported by ceramic tubes inserted half of the bed radius into the combustor. The thermocouple junctions are bare and exposed to the gases of the bed. The precision of these measurements is estimated to be ± 0.5 volume % for the gas analysis and ± 2°C for the temperatures.

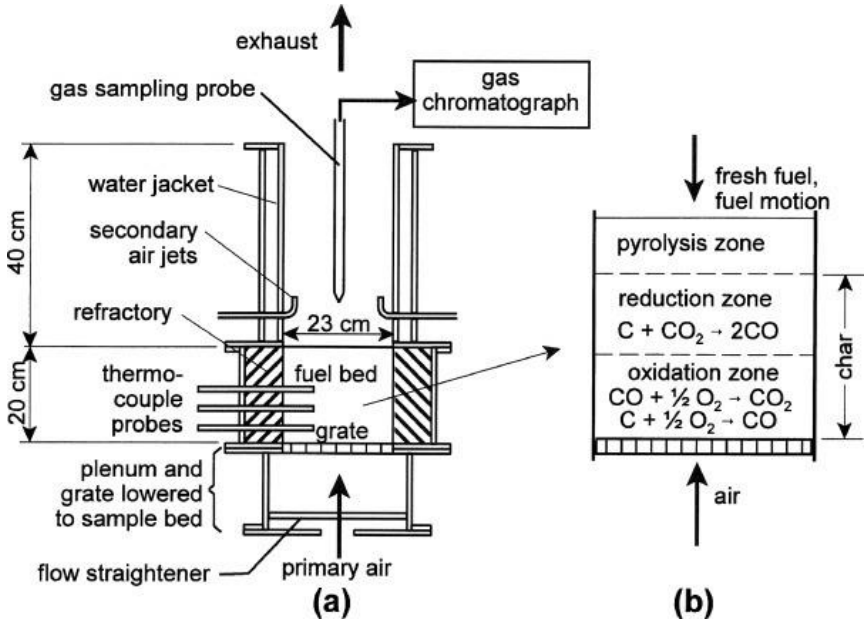

Figure 3.1. (a) Diagram of experimental packed bed combustor. (b) Schematic of reaction zones in the bed

The operation of the combustor is in an overfeed mode: fuel particles are consumed and move downwards against the direction of the primary air; and fresh fuel particles are sprinkled onto the top of bed at frequent intervals from a distance of 40 cm above the bed to maintain the bed level at 20 cm of height. The experiment is started by placing a thin layer of particles on the grate and igniting them with a propane torch. After ignition of the particles, more fuel is added until the bed reaches the desired level. After 45 to 60 minutes the bed reaches quasi-steady temperatures, and the measurements begin at 60 minutes. A completely steady-state can never be reached, since there is gradual ash accumulation on the bed grate, hence the word "quasi-steady". An identical protocol is followed for each test in order to facilitate comparison between different trials: gas analyses are taken at intervals of 10 minutes, normally two measurements at the same height, starting at 1 cm, then the sampling probe is moved upwards to 2 cm, and so on in 2 cm increments until a height of 12 cm is reached. Measurements are not taken beyond this point on account of the danger of fouling of the probe by tar. Previous measurements in the bed had found CO, N_2, O_2, CO_2, and CH_4, the last being a product of devolatilization (Hallett et al., 2013; Trudel et al., 2018). This work will only concentrate on the combustion zone, therefore CH_4 will only occur in small quantities, if at all. All the other species occur and are also measured directly by the gas chromatograph, except for CO_2, which was calculated with mass balances. This approach is used to speed up the

measurements: CO_2 is the last gas to be detected and it normally takes roughly 10 more minutes to read its value. Therefore, instead of one measurement per height above the bed grate, this work can provide two of them.

Careful tamping was occasionally done on the combustor bed, using a steel rod bent into an "L" shape at the bottom, in order to avoid bridging and channel formation. Only a small force – estimated at 200g - was used during the tamping of the bed so that the bed was not compacted. Two replicate experiments were done for each of the particle types.

At the end of the experiment, usually 3 hours, the bed is quenched by substituting a nitrogen flow for the primary air. This will stop char conversion immediately, although the pyrolysis process continues until the bed is sufficiently cooled. From observation of the smoke from the bed, it was noticed that pyrolysis finished within one minute of the start of quenching, at temperatures of about 600°C.

The primary air flow rate was measured with a rotameter and was maintained constant at 3.90 ± 0.5 kg/h. The air entered the combustor at 23 ± 2°C at ambient pressure, which varied between 99.9 to 100.6 kPa.

3.2.2 Fuel Particles

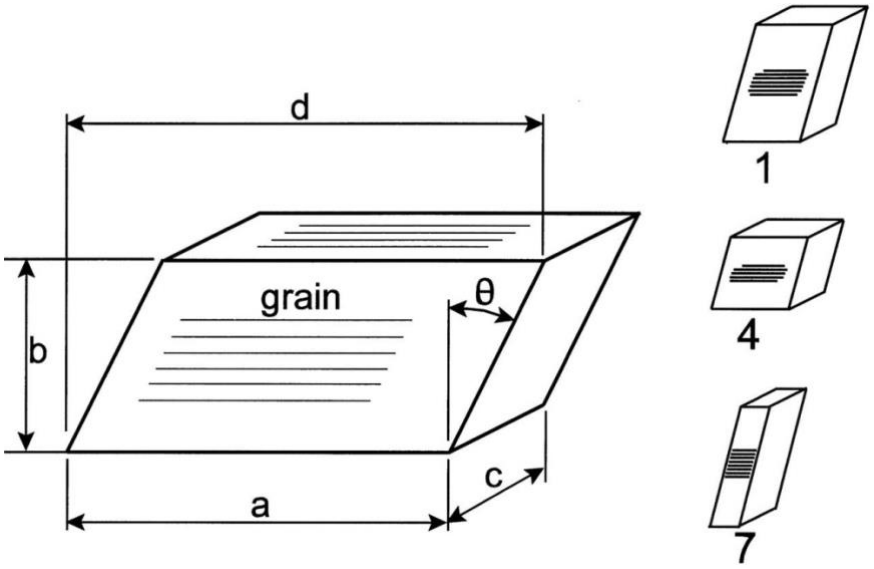

Figure 3.2. Fuel particle geometry. Horizontal line indicates the wood grain direction. On the right-hand side individual particles shapes are shown.

The fuel consisted of Canadian spruce lumber of roughly 16 x 40 mm size, cut with a bandsaw into parallelepipeds as Figure 3.2 shows. Figure 3.2 also provides the direction of the grain, which is important when considering the consumption of the particle and will be further discussed in the Governing Equations section. The reason for the angular shape is that it yields a randomly arranged packing, as can be seen in Hallett et al. (2013). Three particle types of different shapes were used, chosen to give different sizes and sphericities and to produce a packed bed with different void fractions ε as in previous work (Trudel et al., 2018). A Vernier caliper was used to measure the fuel particle dimensions so a calculation of equivalent particle diameter and sphericity Φ could be done. The calculations of volume and surface area included a compensation for the rounded corner of the original wood strips (corner radius of 3 mm). The particle dimensions are displayed in Table 3.1. In this table the effect of the sphericity can be clearly perceived: particles 4 and 7 have a similar size but their sphericities are very different from one another, and the higher sphericity particle generates the packing with the lowest void fraction. The end grain proportion ζ represents the fraction of the particle that has "end grain" surface area over the whole particle surface area. It was first included in the model of Trudel et al. (2018), where it was observed that

the char conversion may occur at different rates in the surfaces parallel to the wood grain direction ("side grain") and normal to the grain direction ("end grain").

Additional information about the particle types and their packings is given by Table 3.2, while proximate analyses and densities of the fuel particles are shown in Table 3.3. The proximate analyses were carried out with dust collected from cutting of the particles with the bandsaw, since all the three different particle types come from the same material. The ASTM standards D3172 – D 3175 and E870 – E 872 were used as the basis of the proximate analyses in this work, though the procedures were not exactly the same. Our test comprised three different parts. The first one, the moisture test, consisted in putting roughly 1 g of sample in the form of small particles in a porcelain crucible, which was then weighed with the lid on. To find the moisture content of the sample, the lid was removed, and the sample was placed in a furnace at 110°C for 1 hour, to be immediately covered with the lid and weighed. The weight difference was the moisture content. The volatiles test was done next: with the lid on the sample was heated for 8 minutes in a furnace at 950°C. This step drove out the volatiles, and after the crucible had sufficiently cooled, it was weighed, and the difference in weight between this and the previous weight was the volatiles content. The ashing test was the last procedure and allowed the measurement of ash and char contents. With the lid off, the sample was heated in a furnace at 600°C for 2 hours, with the furnace door left slightly ajar so that air could enter to ensure combustion of the char. After the two hours, the lid was replaced, the sample was cooled down, and it was weighed again. The heating process with the lid is repeated for one more hour, and sample was weighed again with lids on. If the weight after the two hours process was different from the weight after the last hour, this last step was repeated. If not, the current weight of sample minus the crucible weight was the ash content, and char content could be found by mass balance.

Table 3.1. Fuel Particle Dimensions (before combustion).[1]

Particle	Trial	a (mm)	b (mm)	c (mm)	θ (°)
1	1, 2	17.7 ± 0.3	36.0 ± 0.3	18.0 ± 0.9	19.9 ± 0.6
4	3, 4	17.3 ± 0.3	18.2 ± 0.7	18.1 ± 0.5	20.6 ±1.8
7	5, 6	7.4 ± 0.3	35.6 ± 0.4	18.0 ± 0.2	19.7 ± 0.8

[1] Given as mean and standard deviation of sample of 14 particles or more.

Table 3.2. Particle and bed characteristics prior to combustion.

Particle	Trial	d_p (mm) [1,2]	Φ [1,2]	ζ [1]	η	ε^3
1	1, 2	27.9 ± 0.5	0.763 ± 0.002	0.404	0.79	0.467 ± 0.010
4	3, 4	22.1 ± 0.5	0.799 ± 0.003	0.344	0.81	0.425 ± 0.007
7	5, 6	20.7 ± 0.3	0.638 ± 0.009	0.609	0.80	0.558 ± 0.009

[1] Compensation for rounded corners (3mm corner radius) included.

[2] Given as mean and standard deviation of sample of 14 particles or more.

[3] Mean and standard deviation of 6 different packings.

Table 3.3. Fuel properties before combustion

	Proximate analyses – mass % - as fired[1]				Density[2] (as-fired) kg/m^3	Burning rate kg/hr^3
Trial	Moisture	Volatiles	Fixed C	Ash		
1, 2	8.4 ± 0.7	78.5 ± 1.0	12.8 ± 0.2	0.3 ± 0.2	543 ± 24	3.52
3, 4	8.4 ± 0.7	78.5 ± 1.0	12.8 ± 0.2	0.3 ± 0.2	535 ± 28	3.62
5, 6	8.4 ± 0.7	78.5 ± 1.0	12.8 ± 0.2	0.3 ± 0.2	550 ± 46	3.78

[1] Proximate analyses are given as mean and standard deviation of 6 samples. Results are the same for all trials since the fuel used was the same.

[2] Densities are mean and standard deviation of 14 particles or more.

[3] Averaged over trial, start-up transient time excluded. Average of 2 trials.

3.2.3 Particle Overlap Measurement

The surface area availability η represents the ratio of surface area of the particle in contact with the flow to the total particle surface area. In the cases where particle surfaces are convex, such as spheres and crushed rocks, the surface area availability will be 1 or 100%, while concave or flat surfaces, like the ones in this work, present overlap, thus reducing the area in contact with the flow. Surface area availability η was estimated from analysis of the photos of a bed of unburnt fuel particles through the wall of the bed, similarly to what was done in Trudel et al. (2018) and in

Trudel & Hallett (2017). The container used in the surface area availability measurements is a Plexiglas vessel of identical diameter to the combustor. Packings of the three particle types were analysed separately. Figure 3.3 shows an example of the photos used in the estimation of availability. The estimation process is as follows: particles are numbered in the photos, and for each particle the fraction of each surface covered by another particle is estimated and entered in a spreadsheet. The total area covered is then added up and divided by the total particle surface area. Between 83 and 96 particles from 3 to 4 photos were evaluated for each particle type. This particle overlap was multiplied by 1.5 to account for the normal direction that is not visible and therefore not included in the visual estimation. This method and factor for evaluating particle overlap had been developed and tested in earlier works, as detailed in Trudel & Hallett (2017) and Hallett et al. (2019). Estimation of particle overlap was not done for char particles from the burned bed, since the sampling of the packed bed combustor did not allow both transportation to the transparent vessel and preservation of bed structure simultaneously, and once the bed had been filled with wax it was no longer possible to see overlapping particles.

3.3 Void Fraction Measurement

In works preceding this (Hallett et al., 2013; Trudel et al., 2018), the void fraction had been assumed to be constant and to equal that of the unburnt particles throughout the bed height, as this is a standard assumption for packed bed modelling, except as modified by the accumulation of ash in the voids (Ryan & Hallett, 2002). The measurements of the unburnt void fraction are repeated in this work for the three different particle types and the void fraction for each of them is shown in Table 3.2. A Plexiglas vessel of the same diameter as the combustor (so as to reproduce any wall effects occurring in the combustor) is filled to the top with particles by dropping particles from a scoop above the top of the transparent vessel. The top of the bed was defined as $(d_p/2)$ below the height of the topmost particles as means of roughly correcting the packing anomaly at the top of the bed: the reasoning is that the bed voids at the top surface would be filled by half particles if the bed was higher. The mass of the particles in this bed is measured, and the volume of particles estimated using the density as determined from a sample of 14 or more particles (Table 4.3).

Figure 3.3. Photograph of bed of No. 4 particles

During combustion trials the bed was fed by dropping particles from the top of the combustor at a distance of about 40 cm above the bed surface, and this process was duplicated in the void fraction and particle surface availability tests in the Plexiglas vessel in order to achieve the same random packing.

3.4 Bed Sampling

Although some previous works have used packed beds with the capability of sampling the bed after a combustion or gasification test, the bed sampling procedure used is not always described. Moreover, for packed bed combustors this appears to be the first time the technique described here has been used therefore this section deals with the method used to determine the void fraction of the bed of burned particles after a combustion experiment. The new approach to find the void fraction can be divided into four processes: bed sampling, wax pouring, cutting, and image analysis, from which local void fraction within the bed will be found, whose average is to give the bulk void fraction.

The bed is sampled by a procedure which was developed to preserve the bed structure with as little disturbance as possible. Essentially the bed is lowered in stages and wrapped with successively wider bands of cardstock. The process is shown by Figure 3.4, and it begins by lowering the bed to a certain level (a few mm down) where the end of the upper part sits just on top of the bed grate so a metal slide can be carefully inserted to hold the bed. After this procedure, the grate is continuously lowered until there is enough space to place a shallow pan of card 1.5 cm in height and of same diameter as the grate on top of the grate. At this moment, the metal slide is removed and the bed falls 1.5 cm into the pan. The bed is then lowered in further steps of 1.5 – 2 cm, and at each step a strip of cardboard of progressively greater height is wrapped around the bed and fixed with tape, so particles do not escape as the bed is being lowered, until the final height of the bed is reached represented by the stage “final look” on Figure 3.4.

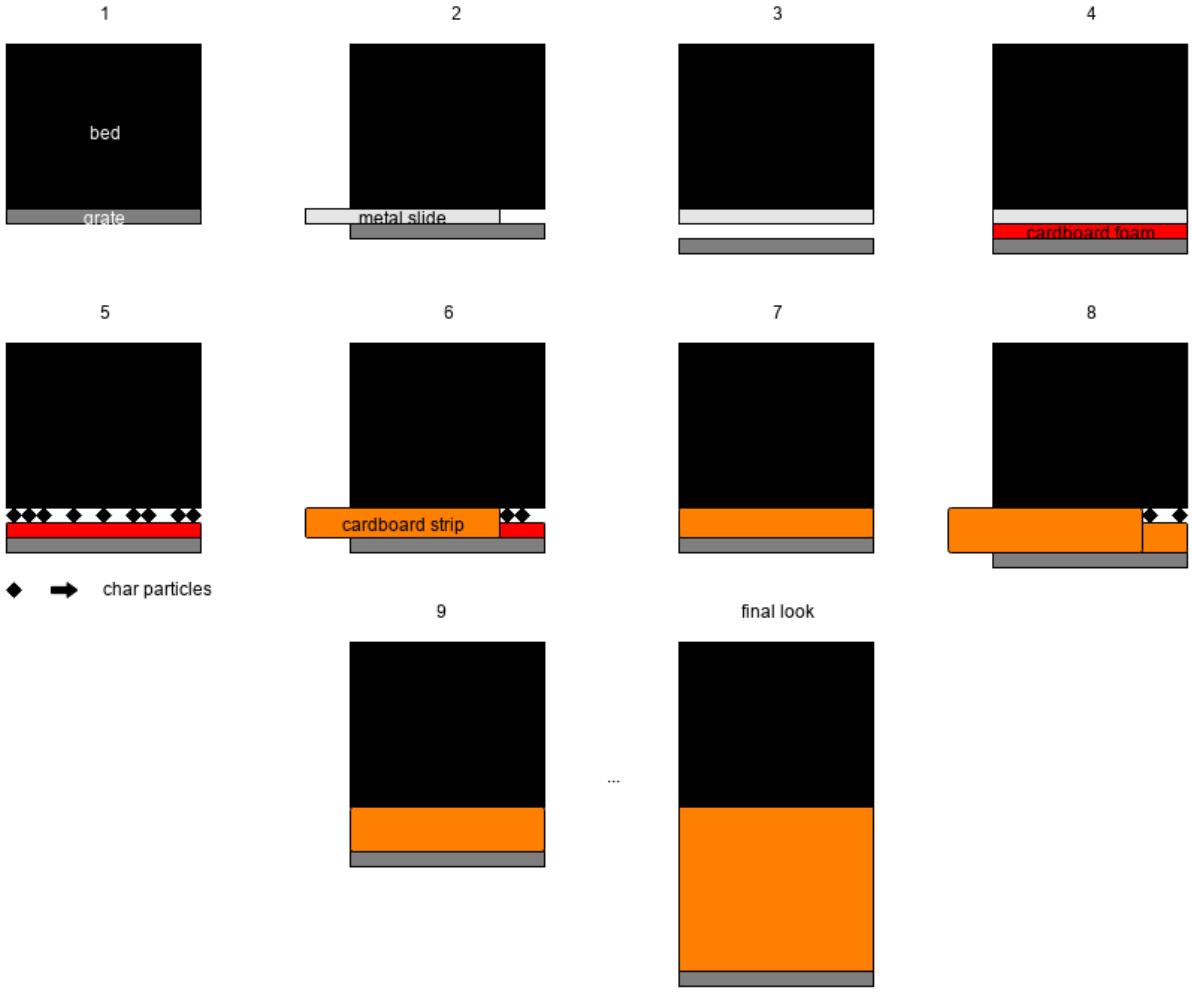

Figure 3.4. Schematic of the combustor bed sampling

After transporting the sampled bed to a lab bench, liquefied paraffin wax is mixed with a red pigment and poured into the packed bed to immobilize the particles and allow the cutting of the bed. Red pigment enhances the contrast with both the unburnt fuel and the char particles and facilitates the image analysis process. The "frozen" bed has now the shape of a cylinder, and is cut. Several cuts with a handsaw at different heights are done in each bed parallel to the base of the bed in order to produce slices, so two radial cross sections are generated per slice, one on each side of the saw cut. Finally, photographs of these radial cross sections are taken, and through an image analysis software named *ImageJ* (n.d.) the photographs are binarized and the void area is estimated, as described more carefully in Section 4.2. Since the correlation of the void cross-sectional area

and the void volume of a bed is mathematically exact (eq. 2.1, Section 2.2), one can state that the void area fraction on a cross section is equal to the local void volume fraction. Finally, the bulk void fraction of each bed can be found by averaging all the local void fraction measurements at different heights. The saw cut had a width of 2 mm, consequently the cross section on either side of the cut could give different values of void fraction, so opposite sides (cross section) of a single cut in the bed were averaged between themselves prior to calculating the bulk void fraction. This procedure would, therefore, avoid that opposing sides of a cut had a greater influence on the bulk void fraction calculation. In some cases, only one side of a cut could be analyzed, and this procedure avoided reducing the weight of such cuts in the average.

In order to analyse the radial cross section profiles for each packing, the cross sections are divided into a number of annular rings and the void fraction estimation is done for each of these rings, similarly to what has been done by Hamel & Krumm (2008). Each ring has the same radial difference of 0.1 relative radius (r/R). The position of each measurement is then given as an average of the smaller and bigger radius of the annular ring: for example, the closest measurement to the wall is located between 0.9 and 1 relative radius, so their average (0.95) would be the position of its measurement. A total of six measurements, one for each ring, were made for each cross section, varying from 0.95 to 0.35 of the relative radial position, since as smaller the ring radius gets less representative is the area covered by the ring which would cause the void fraction to tend towards 0 or 1, and it's far enough from the wall so this could not be affected by the wall effect. At the centre, instead of dividing the area into smaller rings, it was decided to analyze the void fraction of the area inside a circle of 0.3 relative radius in order to have an area that was large enough to be representative.

3.5 Image Analysis

Before being binarized the colour image of the cross section is treated so as to produce a greyscale image. After that procedure is completed the binarization takes place, where the threshold chosen for this process is based on intensity, not colour. The software automatically chooses a threshold but a finer adjustment is made so the binary image is a true representation of the coloured image. The finer adjustment consisted of two processes. First, images were compared side by side – colour images with binarized ones – and checked to see if the smaller voids between the particles had

approximately the same size after binarization. This check was also done for the smaller sized particles. Secondly, colour images were superimposed on binary images to check if they correlated in void and occupied space, and then the threshold was adjusted until there was good agreement. The automated choices of threshold by the software were changed by up to only 3 units, in most cases up to half of that, which can be seen in the following discussions to not change the void fraction significantly. To evaluate the effect of selecting different values of the threshold for a cross section on the local void fraction, a plot of threshold vs void fraction is displayed by Figure **3.5** - Figure **3.7**, where one representative cross section is chosen for each particle packing, i.e. one packing of each particle type. The local void fraction of the selected cross section as found after the fine adjustment mentioned above is presented with a line across the graph, and the threshold values can vary from -8 to 42, -5 to 35, -11 to 37 respectively for the cross sections analyzed at Figure **3.5** -Figure **3.7**. Only the threshold values around the actual chosen one are presented here, since these are the ones that would most likely to be mistaken.

The cross sections of the analyzed images present an average of pixel count of around 670,000 pixels, and to address the accuracy of the image analysis, one would wonder what the difference in the measured area fraction would be if the boundary of a particle was displaced by one pixel. This is not a straightforward calculation, since it depends on the shape of particles encountered on the cross sections, and how many they are. Supposing the void fraction is around 35%: this would represent a total of 234,500 pixels in our case. A test was performed in which 40 spherical particles were placed in area of the bed cross-section with a void fraction of 0.35. Displacement of the particle boundary by 1 pixel outwards for each of these particles would decrease the void fraction to roughly 33% - a change of 0.02. This number of particles was similar to the number of fuel particles in a typical cross-section, and therefore gives a realistic estimate of the sensitivity of the results to uncertainties in particle boundary definition.

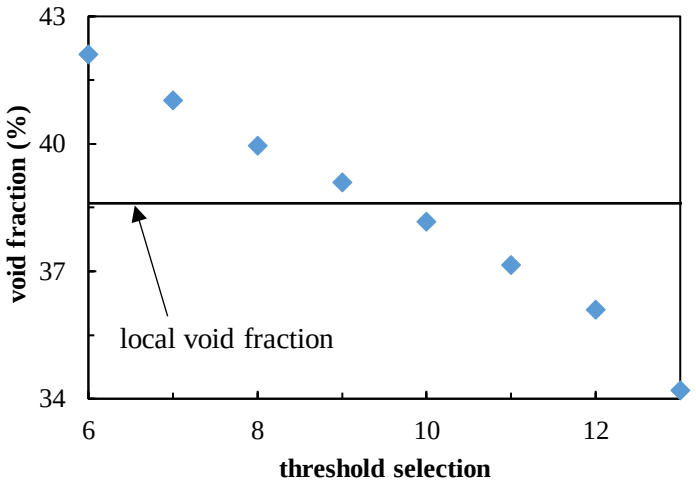

Figure 3.5. Sensitivity of void fraction with different thresholds. Experiment 2 - x/H = 0.31

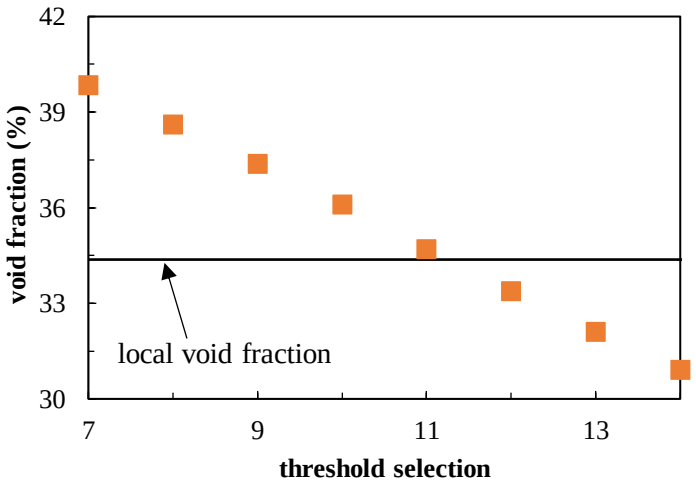

Figure 3.6. Sensitivity of void fraction with different thresholds. Experiment 3 - x/H = 0.26

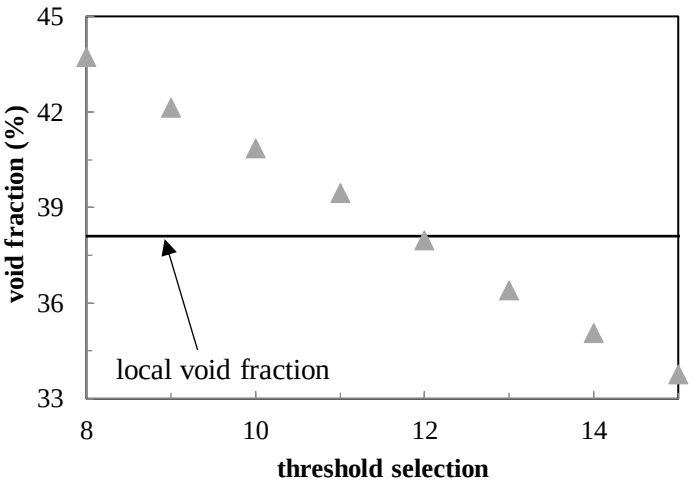

Figure 3.7. Sensitivity of void fraction with different thresholds. Experiment 5 - x/H = 0.75

An example of an analysed radial cross section is shown by Figure 3.8. The difference in void fraction between the binarized particle by a threshold of 10.5 and the one by a threshold of 13.5 is roughly 3%, and visually, parts of either cross sections are distinguishable.

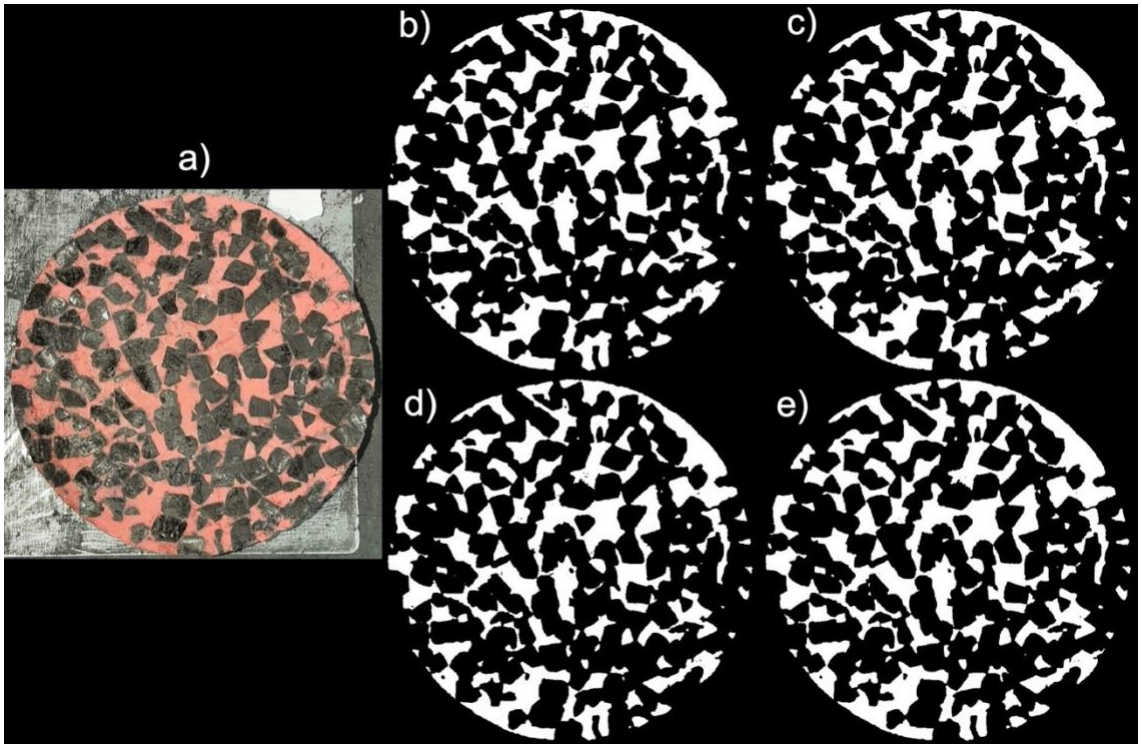

Figure 3.8. Example of a colourized radial cross section and binarized by different threshold. a) Original; b) Binarized – Automatic threshold (12.04); c) Binarized – Adjusted threshold (11.85); d) Binarized – threshold of 13.5; e) Binarized – threshold of 10.5.

In order to ensure accurate estimations of bulk void fraction, a packed bed of unburnt particles was formed and the same photograph analysis methodology used in the post-combustion packed bed was used here. The particles used in this test were very close to particle type 2 presented in the study of Trudel & Hallett (2017), and the bulk void fraction of the packing with this particle type is 0.443 ± 0.06 as given in that paper. By the use of image analysis and averaging the void fraction from different cross sections of the bed, the bulk void fraction found was 0.429, which deviates by less than 4% from the original value, which indicates that the use of image analysis for the burnt particles should be accurate. This comes as previously noted in this work, that if a cross-section is taken of a packed bed, the void volume fraction will be equal to the fraction of void area seen in the cross-section. The void volume in a slice of thickness dx is given by eq. (2.1), which by definition gives the bulk void fraction ε of the total volume V. This definition is important because it allows the estimation the void fraction of a packed bed by averaging fractions of void areas.

4.1 Introduction

Numerical simulations of the experimental tests were performed in order to assess the effects of the new findings of void fraction in a packed bed on the combustion model outputs, such as temperatures and species concentrations.

4.2 Governing Equations

The numerical model presented in this work was first introduced by Cooper & Hallett (2000), and has been thoroughly tested against a large number of experiments with different particle shapes and fuels (Ryan & Hallett, 2002,Girgis & Hallett, 2010, Hallett et al., 2013, Trudel et al., 2018). The reason behind the selection of this model is that it is complete and includes all relevant phenomena of packed bed combustion, and it has been tested against experiment. The model was used without any significant alterations, the only change proposed here being the introduction of a variable void fraction, instead of the original fixed one. It is a one-dimensional (quantities vary only in the vertical coordinate direction) transient solution of the governing differential equations of energy, mass and species conservation in both gas and solid phases, solved by finite volume techniques to give details on temperature, particle properties and gas and solid composition as functions of time and position. The governing equations are differential mass and energy balances on the solid and gas phases; details are given by Cooper & Hallett (2000). The continuity equation for the solid phase is:

$$\frac{\partial}{\partial t}[(1-\varepsilon)\rho_s] + \frac{\partial}{\partial x}(\rho_s v_s) = -Ga_B, \tag{4.1}$$

where G is the carbon conversion rate per unit particle surface area and v_s is the superficial velocity of the solid phase in bulk. This equation is solved for the solid mass flux ($\rho_s v_s$). The continuity equation for the gas phase is:

$$\frac{\partial}{\partial t}(\varepsilon\rho_G) + \frac{\partial}{\partial x}(\rho_G v_G) = Ga_B, \tag{4.2}$$

while for the individual species i (i=CO_2, CO, or O_2),

$$\frac{\partial}{\partial t}(\varepsilon\rho_G Y_i) + \frac{\partial}{\partial x}(\rho_G v_G Y_i) = \frac{\partial}{\partial x}(\rho_G D_{ieff}\frac{\partial Y_I}{\partial x}) + \varepsilon r_i. \tag{4.3}$$

The energy equation for the solid phase is

$$\frac{\partial}{\partial t}[(1-\varepsilon)\rho_s h_s] + \frac{\partial}{\partial x}(\rho_s v_s h_s) = \frac{\partial}{\partial x}(k_{Seff}\frac{\partial T_S}{\partial x}) + h_{SG}a_B(T_G - T_S) + Ga_B\Delta H_{RC}. \tag{4.4}$$

All the heat ΔH_{RC} generated by the solid surface reactions is assumed to be first deposited in the solid phase. The energy equation for the gas phase is:

$$\frac{\partial}{\partial t}(\varepsilon\rho_G h_G) + \frac{\partial}{\partial x}(\rho_G v_G h_G) = \frac{\partial}{\partial x}(k_{Geff}\frac{\partial T_G}{\partial x}) - h_{SG}a_B(T_G - T_S) - \varepsilon r_{CO}\Delta H_{RCO}. \tag{4.5}$$

Separate energy equations are required for the gas and solid phases. As particles are consumed and move downwards, a further balance equation is needed to account for changes in particle size. The required transport equation is derived from a particle number balance equation on a horizontal slice in the bed (Cooper & Hallett 2000):

$$\frac{\partial}{\partial t}[\frac{(1-\varepsilon)\rho_S}{m_P}] + \frac{\partial}{\partial x}[\frac{\rho_S v_S}{m_P}] = 0. \tag{4.6}$$

The overall rate of char conversion at the particle surface G is determined by a competition between mass transfer and reaction kinetics.

A competition between mass transfer and reaction kinetics determines the overall char conversion at the particle surface, where the total flux of a certain specie must match the rate production of this specie in the bed at the char surface. With the temperatures encountered in this work, the product produced by the oxidation reaction is almost exclusively CO.

For carbon oxidation an equation derived for low-rank bituminous coal char was employed:

$$G_{R1} = A_{CO} p_{O_2} \exp\left(-\frac{E_{CO}}{RT_S}\right). \quad (4.7)$$

The rate constants used here may differ for different chars from different fuels, but since char oxidation proved to be largely diffusion-controlled rather than kinetically, this has little consequence. For the reduction of CO_2 by char the following correlation was used:

$$G_{R2} = A_{CO_2} p_{CO_2} exp\ (-\frac{E_{CO_2}}{RT_S}), \quad (4.8)$$

where the rate parameters A_{CO_2} and E_{CO_2} were chosen to give the best agreement with the data and are shown by Table 4.1. (Trudel et al., 2018). A one-step equation was used to model the gas phase oxidation of the CO leaving the particle surface to CO_2, while a reverse reaction was added to account for the dissociation of CO_2 at high temperatures (Cooper & Hallett 2000).

The notation for the terms in the fundamental equations is defined in the original work of Cooper & Hallett (2000). The governing equations were solved for gas and solid mass fluxes and temperatures, CO_2, CO, and O_2 mass fractions and particle masses using finite volume methods, as detailed by Cooper & Hallett (2000). The grate was also included in the calculation grid, the only difference to the solution for the bed is that v_S = 0. The results presented here were all produced by running the model for the duration of the experiment, so that the output at the final time would represent the bed sample.

Wood pyrolysis was represented by a single step pyrolysis reaction with rate constants as given by Trudel et al. (2018). This is a simplified treatment of pyrolysis, but in this study the main function of pyrolysis is only to provide char for consumption in the lower part of the bed. Since the pyrolysis zone is located downstream from the char conversion zone, its influence on the char conversion zones is not significant.

Pyrolysis of fresh fuel occurs at the top of the bed and it is assumed to occur at a constant particle volume and decreasing density, while char is modelled as constant density and decreasing size. The assumption of a constant sphericity throughout the bed is supported by previous experimental results (Trudel et al., 2018).

The calculation domain for the model comprises 80 evenly-spaced points in the bed and an additional 10 points for the bed grate, the results that interest this work start at the top surface of the bed grate. A time step of 1 s is applied.

Reaction rates as well as other input parameters needed for the model simulation are provided by Table 4.1.

Table 4.1. Reaction Rate and Model Input Parameters

Reaction or property	Rate or value
Volatiles composition (% by mass of total dry volatiles)	35% CO, 10% CO_2, 6% CH_4, 49% tar
Emissivity	0.8
Ash diameter	0.1 cm
Ash density	1030 kg/m^3
Ash void fraction	0.45
Ash sphericity	0.6
Ash layer	10 cm
$C + CO_2 \rightarrow 2CO$	$A_{CO_2} = 0.06\ kg/m^2\ s\ kPa$, $E_{CO_2} = 200\ kJ/\ gmol$
$C + 0.5O_2 \rightarrow 2CO$	$A_{CO} = 0.86\ kg/m^2\ s\ kPa$, $E_{CO} = 18\ kJ/\ gmol$
Pyrolysis	$r_P = \xi_V \rho_{F0} A_P Y_W \exp(-E_P/RT)$ (kg pyrolysis products / (m^3 solid s)); $A_P = 0.02\ s^{-1}$, $E_P = 20$ kJ/ gmol; Enthalpy of pyrolysis 300 kJ/kg (endothermic)
Particle pore characteristics for CO_2 reduction	$\varepsilon_P = 0.6, \tau = 1, a_I = 3 \times 10^7$ m^2/m^3 particle volume

Fuel particle shape effects include accounting for particle overlap and wood grain direction as detailed by Trudel et al. (2018). The effect of particle overlap was introduced in the model by means of the parameter η (see Section 3.2.3 for reference), which is multiplied by the specific surface area of fuel particles in the bed, while the wood grain direction was accounted for by introducing an effective reaction rate that is dependent on the end grain proportion ζ. The end grain was assumed to have a reactivity for the CO2 reduction reaction five times larger than that for the side grain, as in earlier work (Trudel et al. 2018).

Chapter Five: Results and Discussion

5.1 Introduction

This chapter presents the results for the void fractions in a packed bed combustor obtained by image analysis of radial cross sections as well as local and averaged void fractions for each of the three different packings. Also shown are comparisons of the measured temperatures and gas concentrations calculated with the numerical combustion model.

5.2 Radial Void Fraction Profile

Individual radial profiles obtained at different heights of the bed for the char samples from the burned bed are displayed by Figure 5.1 to Figure 5.3, each of which is for a different particle type: 1, 4 and 7. The void fraction of the rings closer to center of the bed was not measured, since as the ring radius gets smaller, the area covered becomes too small to be representative, so void fraction values would tend towards 0 or 1. Moreover, as one moves closer to the centre the void fraction will be likely be more constant, as no wall effect should be present.

For particle type 1 (Figure 5.1) the void fraction profile with the most variation was located around half of the bed height, at 0.45 relative axial position, showing that the void fractions near the bottom and top of the bed did not present as much variation, and this is important in addressing channelling effects. This variation for the 0.45 relative height was mainly due to the wall effect: nearer the wall of the bed this cross section presented a void fraction 37% higher than the average of this cross-section's void fraction in this chart and 58% higher than the average of all the cross sections. It is important to define that the average over the cross section here is a weighted average with the area, therefore the rings closer to the wall will have greater impact in this average. Particle type 4 (Figure 5.2) like particle type 1, exhibited the same effect of a cross section having the most variation and the largest wall effect of all; this was for the cross section at 0.74 relative height, where the void fraction at the nearest point to the wall was 47% higher than that of its averaged cross section and 42% higher than the average of all the cross sections. Finally, particle type 7 (Figure 5.3) showed a similar trend to particle 4: the cross section located at the topmost position (0.79 relative height) presented both the highest variation and highest increase in void fraction near

the bed walls, with a value 52% higher than the average of the cross section at the same position and 84% higher than the average of all cross sections. Results of particle type 7 radial distribution may indicate an increased likelihood of a channelling to occur in a region of the bed: at two sequential layers of relative heights of 0.76 and 0.79, in both radial positions 0.85 and 0.95 it can be seen that the void fraction are higher than the void fraction of other axial and radial positions. These results may be important to this study, as the wall effect seems to mostly affect areas in which particles less consumed are present, closer to the top of the bed, and as particles are consumed the wall effect wanes away. In order to contextualize, at locations over 0.6 of the relative axial position, the pyrolysis zone is present, as Figure 5.10 to Figure 5.12 display, so it is suggested that this is the zone most affected by the wall effect.

Although measurements of radial void fraction profiles extended to rings up to 0.35 radial position, a single void fraction measurement of a disk of 0.3 relative radius was measured for each cross section. The measurements of these disks' void fraction displayed a relatively small change in void fraction compared to the average of the rings. For packings of particle types 1 and 4 an increase of 1% and 2% were observed and a decrease for packings of particle types 7 of 6%, likely because of its irregular shape, all compared to the average of the regions from 0.35 to 0.95. Therefore, it can be observed that the centre of the bed presents around the same void fraction than the average of the exterior rings do, and this can ultimately indicate a balanced distribution of particles in the bed radially.

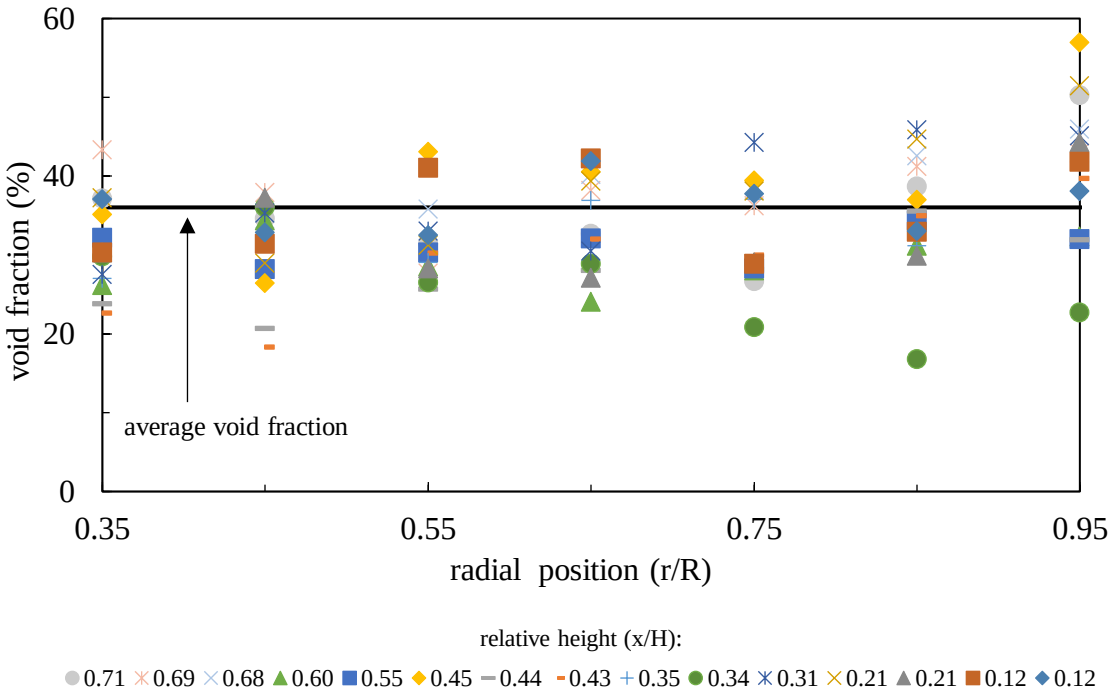

Figure 5.1. Void fraction measurements as function of radial position for each cross section in the beds of particle 1 (experiments 1 and 2).

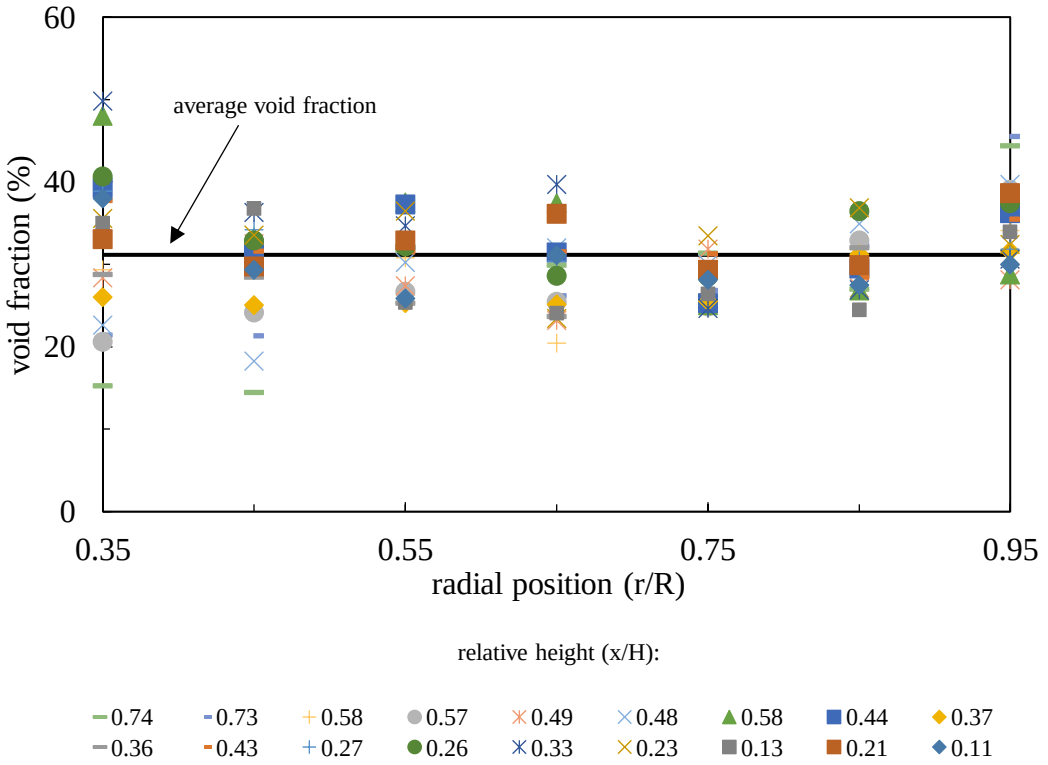

Figure 5.2. Void fraction measurements as function of radial position for each cross section in the beds of particle 4 (experiments 3 and 4).

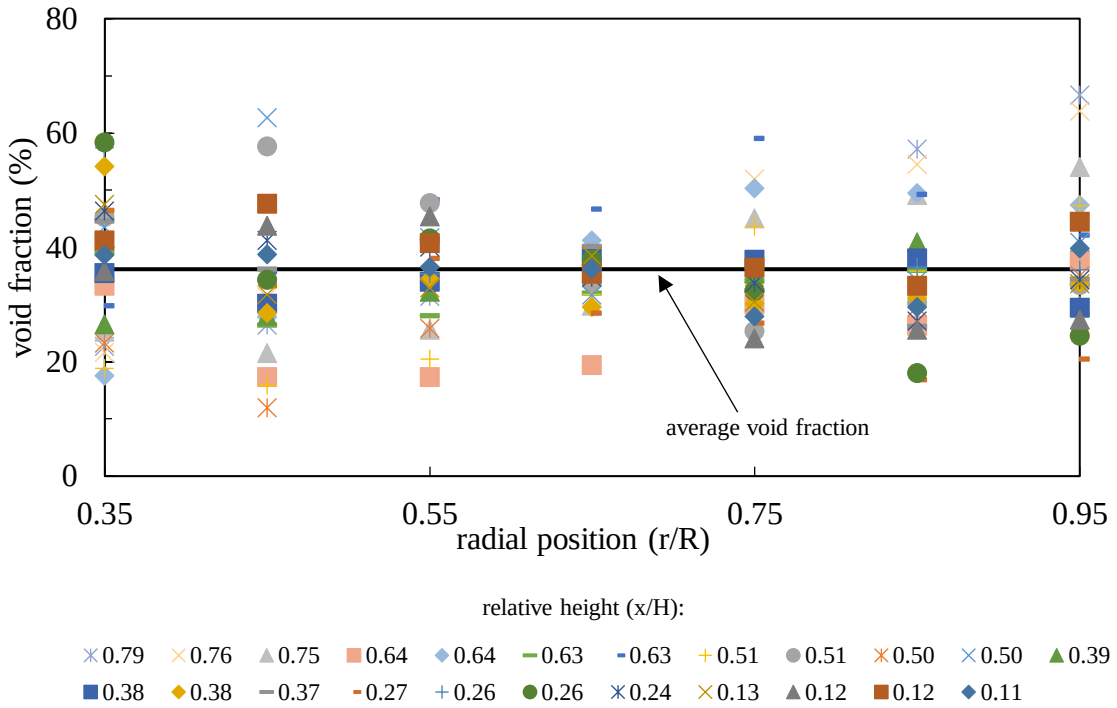

Figure 5.3. Void fraction measurements as function of radial positions for each cross section in the beds of particle 7 (experiments 5 and 6).

The averaged radial void fraction profiles shown in Figure 5.4 to Figure 5.6, as these are the averages of the void fractions at each radial location over the whole height of the bed. The measurement closest to the wall, at a radial position of 0.95 R presents the same trend for all the packings: it is the greatest value of all void fractions found within the bed cross section. This is explained by the wall effect, as particles will tend to pack more loosely because of the presence of the wall which would generate a packing anomaly in this area. This result has also been reported by Hamel & Krumm (2008), Benyahia (1996), Man et al. (2005), and Roblee et al. (1958) to name but a few. The most pronounced wall effect is found for the largest particle type, the particle type 1 (Figure 5.4), as it takes relatively more distance from the wall to reduce the effect. Particle type 4 (Figure 5.5) is the most nearly spherical particle of all, and one can note this characteristic resulting in a more regular packing closer to the wall, so the measurements did not vary much, while as one moves to the centre the standard deviation starts to increase. In the case of particle type 7 (Figure 5.6), its packing presented a high standard deviation not only in the wall vicinity but also closer to the centre of the bed, and this is not a surprise since it is the least spherical particle and has more tendency to pack randomly. The most uniform distribution of mean void fractions is

found for particle type 7 although the standard deviation is also the greatest, and this may come as an effect of smallest particle. The high standard deviation in this is a result of the high standard deviation seen in several cross sections (Figure 5.3), owing to a very random packing characteristic. The flat shape of particle 7 may be responsible for this irregular arrangement: the randomness of the packing increases with this type of shape, as any change in the orientation of this particle type (vertical, horizontal, inclined) causes a big change in the packing structure.

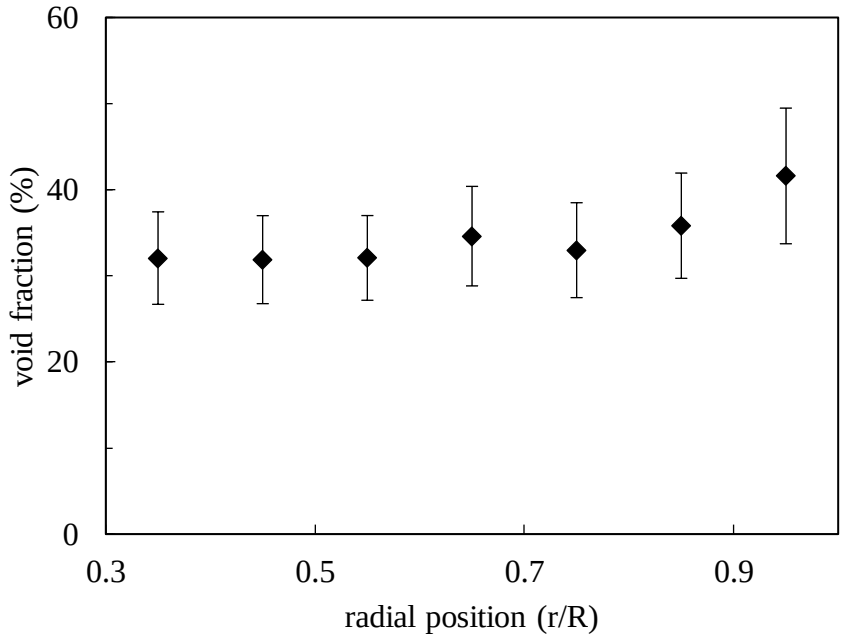

Figure 5.4. Averaged void fractions over the whole height of the bed as function of radial position for particle 1 (experiments 1 and 2). Error bars indicate standard deviation.

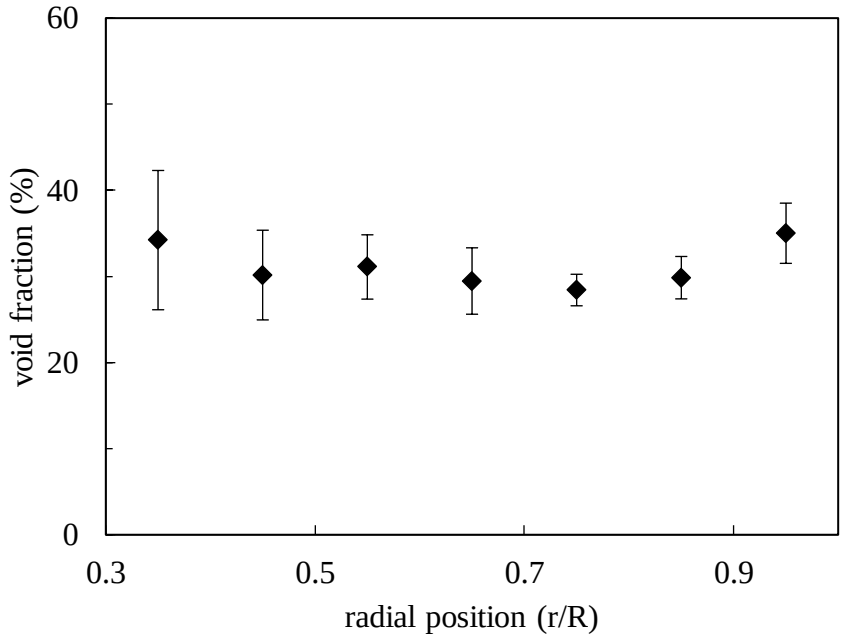

Figure 5.5. Averaged void fractions over the whole height of the bed as function of radial position for particle 4 (experiments 3 and 4). Error bars indicate standard deviation.

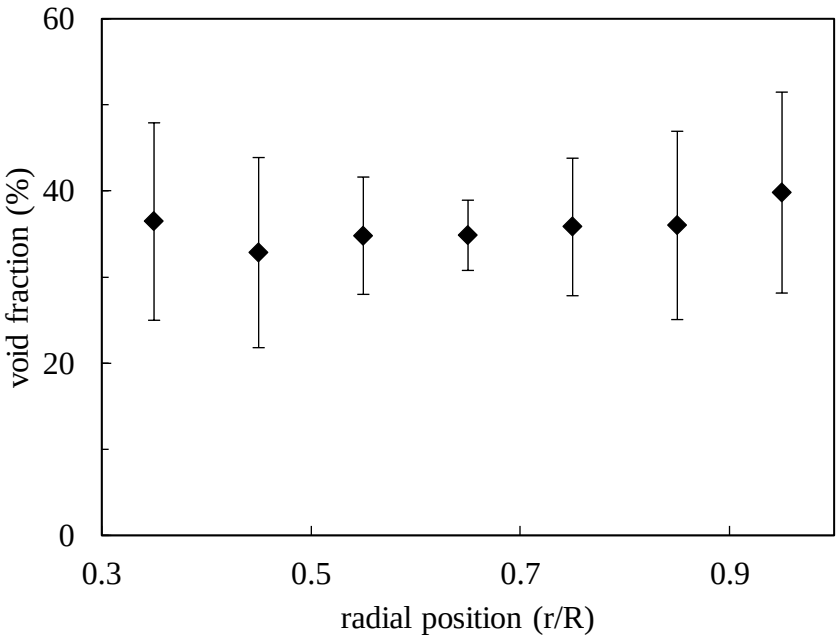

Figure 5.6. Averaged void fractions over the whole height of the bed as function of radial position for particle 7 (experiments 5 and 6). Error bars indicate standard deviation.

5.3 Axial Void Fraction Profile

The axial void fraction profile is the average void fraction at each cross section, plotted at different heights in the bed of char samples. The average at each section was determined by applying image analysis to the entire section, not by integrating the local measurements shown in Figs 5.1-5.3. For each bed local void fraction measurements at different heights were done using an image analysis approach to finally generate the axial void fraction profile of the bed. The profiles of the beds using the same type of particle were plotted on the same graph, therefore three different profiles are plotted, each for each particle type. The axial void fraction profiles are presented in Figure 5.7 to Figure 5.9, they represent the area of voids in a cross section over the area of the whole cross section. The values at the bed top were assumed to be the void fraction of a bed of the unburnt fuel particles for each respective particle, according to Table 3.2; this is reasonable to assume, since unburnt fuel is dumped onto the bed top (relative height of 1).

The graphs indicate that the void fraction in the burned bed is consistently lower than the void fraction of unburnt particles, whereas previous work had assumed void to be constant and equal to that of the unburnt fuel throughout the bed (Hallett et al., 2013; Trudel et al., 2018). This is a surprising finding given findings on the burned particles from previous works, which discovered particles not to vary much in size and shape. Moreover, because the particles are light - they typically have a specific gravity of 0.2 (Trudel et al., 2018) - and due to the small depth of the bed, gravity is not likely to have the effect of crushing the particles thus decreasing the void fraction. As the conversion of the wood and char occurs in the bed, the particles become smaller and their corners become rounded, so that they tend to fill the bed more densely. This agrees with the linear regression fitted, which indicates an increasing void fraction as height above bed grate increases. However, this is only part of the explanation, as the particles go through only a small size reduction. Another factor is fragmentation of particles which may occur from thermal stresses during pyrolysis or combustion. The results of these effects would be smaller particles filling voids between unbroken ones; this may also be part of the explanation of the void fraction reduction. However, only roughly 10% of the particles were broken according to direct observation of the cross section of the bed, and when the bed was sampled, most broken particles were found closer to the bed bottom. Another effect of the packed bed combustion is the tendency in transforming sharp edges in the original particles to more rounded ones, and this may allow particle to pack more closely and help decrease the void fraction: particles with more angle on their edges, like on the

original fuel particles tend to act as a “wall” and force neighbour particles to pack accordingly, therefore the rounding of the edges may avoid this effect and help reduce the local void fraction at this point. Finally, the tamping of the bed, which is done to avoid bridging and channelling, is another possible cause of compaction, although this was done gently in order not to compact the particles.

The frozen bed technique was also used in a packing of unburnt particles of type 2 to test the “freezing” method. Particle type 2 (described in Trudel et al. (2018)) is similar in shape and dimensions to particle 1, with the only difference being that the end grain surface was the smaller area, corresponding to face a-c for Particle 1. The cross section of the burnt beds of particle type 1 also allowed one to infer that the particles came closer to each other, sharing part of their perimeters much more frequently, compared to cross section samples of the unburnt particles of type 2. It would be expected that this effect would be repeated with particle types 4 and 7. This comparison also guided to another qualitative finding: the cross sections of the particle type 1 packing were found to be more random than the unburnt particle type 2 packing. This is likely owing to the movement of multiple particles downward simultaneously as particles are consumed, although a greater randomness was observed near the top of the bed as a greater particle size distribution width is likely located in this region given a higher decrease in particle size (Trudel et al., 2018).

An effect of decreasing scatter in the points with increasing particle sphericity can be observed also in the axial void variation charts when comparing measured data for all particle types (Figure 5.7 to Figure 5.9). For particle 7 (Figure 5.9), one can note that another effect besides this: standard deviation increasing with height above bed grate. This may also be explained by the flat shape of particle 7 as well: closer to the bottom a more stratified structure may be present while farther from it a more random packing structure may take place, as can be seen in Montillet & Le Coq (2001) which used particles similar in shape to the particle 7, although a minor difference can be noted: the ones in their work were not angular as in this work.

No end effect is noticed in the local void fraction measurements for any of the experiments. Two explanations can be given for this. The first is the reduced particle size at the bottom of the bed, which in turn causes a greater effective height-to-particle diameter ratio. The second is the fact that the first measurement in the bed is not very close to the bottom of the bed, being roughly 2 cm of height above grate, owing to experimental difficulties in slicing the bed.

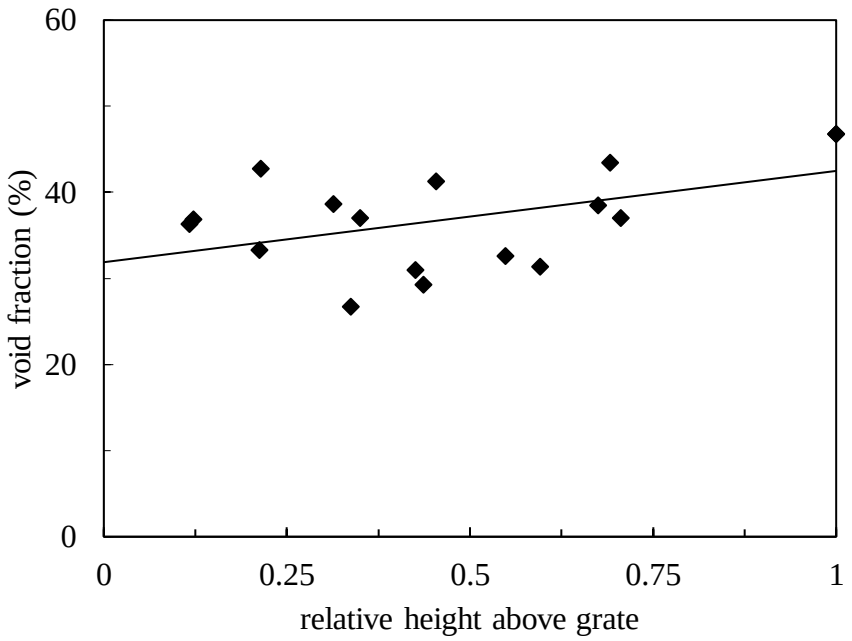

Figure 5.7. Void fractions as function of relative height above bed grate for Particle 1 (experiments 1 and 2). Points are measurements and the line originates from linear regression.

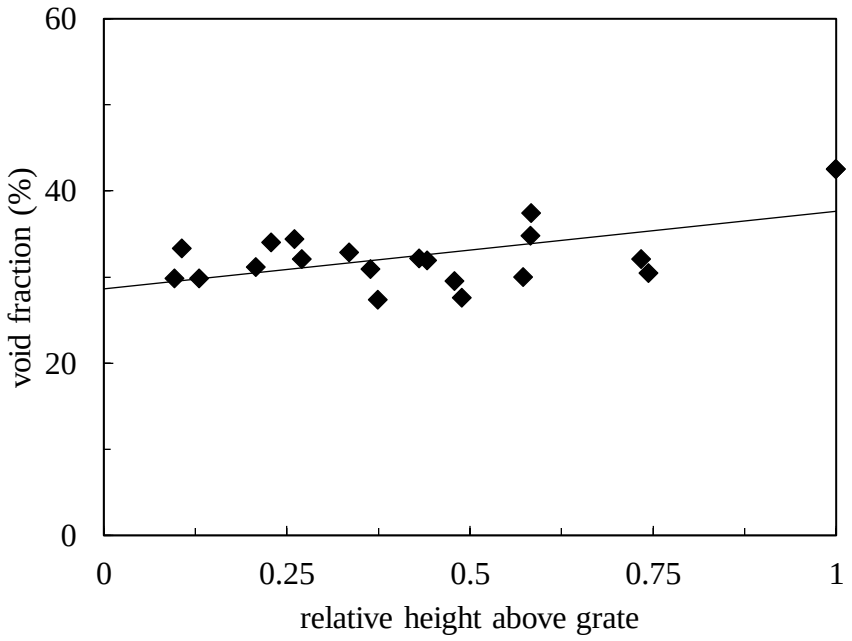

Figure 5.8. Void fractions as function of relative height above bed grate for Particle 4 (experiments 3 and 4). Points are measurements and the line originates from linear regression.

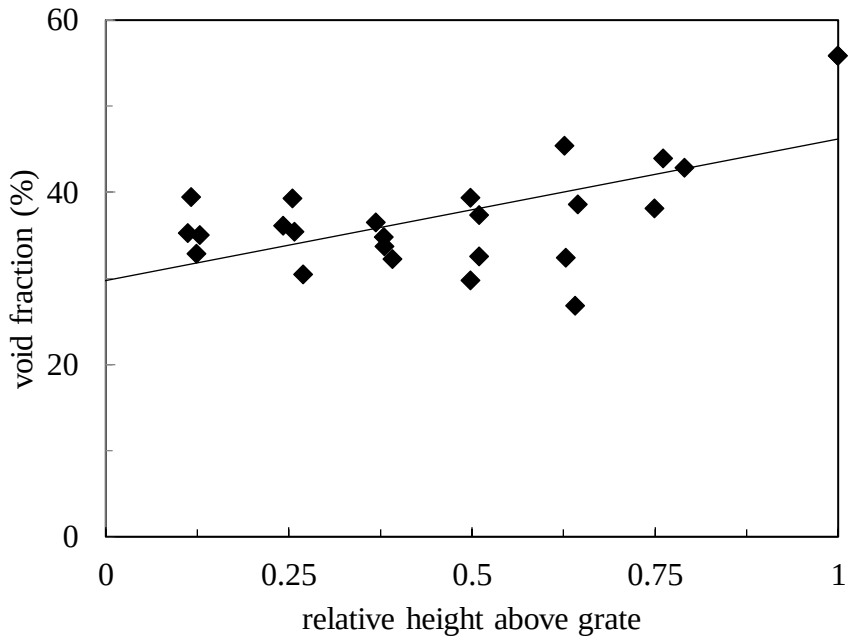

Figure 5.9. Void fractions as function of relative height above bed grate for Particle 7 (experiments 5 and 6). Points are measurements and the line originates from linear regression.

The averaged void fraction of each packing is presented by Table 5.1. These values were calculated by averaging each of the axial void fractions over the whole bed. When the bed was cut into slices, two cross sections could be explored at approximately the same height (not exactly the same because of the saw kerf), each of which represented one side of the cut, and in this case these cross sections were averaged into one so as not to provide a larger weight when averaging the void fraction for the whole bed, given that some of the cuts did not allow observation of two cross section.

It can be seen that the order of highest void fraction was kept the same, as particle 4 is the one that produces the densest packing, whereas particle 7 is the one that produces the loosest packing after the combustion, though the reduction in void fraction of particle 7 due to combustion is the most significant one. This suggests that the shapes of the particles are kept roughly constant during combustion, as previously discussed. This work did not provide any means of analysing the sizes and shapes of whole particles, but previous work (Trudel et al., 2018) shows that the greatest shrinkage of all particles was in particle 7, because this particle has the largest proportion of end grain, and the end grain is consumed much more quickly. The particle 7 of that work has roughly the same size as that used in present work.

Table 5.1. Averaged bulk void fraction from image analysis and comparison with void fraction of unburnt particles

Particle	Averaged Void Fraction from Image Analysis	Relative Difference from Unburnt Particles' Void Fraction
1	37.8%	-19%
4	33.5%	-21%
7	39.0%	-30%

Given the dispersion of the void fractions at each axial position, the development of a mathematical model to represent the variation of void with height became challenging, so a simple linear equation was chosen. Eqs. (5.1) to (5.3) are the equations for the linear regression lines seen in Figure 5.4 to Figure 5.6, respectively, where h is the relative height above the bed grate. One can notice some similarity of these equations with the assumption of Chen & Gunkel (1987), who assumed a linear variation of local void fraction from 0.3 at the bottom to 0.5 at the top in a study on a gasifier. In their work a completely spherical particle was assumed, which may explain the difference between the void fractions at the top.

$$\varepsilon_1(h) = 0.10602h + 0.31885 \tag{5.1}$$

$$\varepsilon_4(h) = 0.09012h + 0.28630 \tag{5.2}$$

$$\varepsilon_7(h) = 0.16441h + 0.29755 \tag{5.3}$$

5.4 Numerical Simulation Results: Gas Concentrations and Temperatures

The numerical model was used to run simulations of each of the packed bed combustion experiments. The purpose of doing this was to test the effects of the different treatments of the void fraction in the bed. Figure 5.10 to Figure 5.15 compare measured species concentrations and temperatures with predictions of the numerical model. The model results in the figures for both volume fraction and temperatures are "composite" curves, in which for a given height above the grate the model prediction that corresponds to the time the nearest gas sample was taken is plotted. This allows a more direct comparison of the model and experiments, since the gas analyses were measured over an extended period of time.

Figure 5.10 to Figure 5.12 show concentrations of CO and CO_2 as functions of height above the grate, excluding the pyrolysis zone (top 6 cm or so) of the bed, for which no measurements were taken to avoid the risk of fouling the sampling probe with tar. Measurements were taken twice for each of the following heights: 1, 2, 4, 6, 8, 10, and 12 cm, except for Trial 6, for which a shortage of fuel left only one measurement at height 10 cm and none at 12 cm. Model predictions actually continue until the top of the bed, but as pyrolysis starts to take place in areas closer to the top, the model predictions will only display the region covered by the measured points. A typical gas concentration curve for overfeed combustion is observed: at the bottom, oxygen is rapidly consumed by char, reacting with the char particle surface and producing CO; however, this CO is rapidly oxidized into CO_2, giving high temperatures and increased reaction rates in the oxidation zone. After the oxygen is completely consumed by the bed, CO_2 reaches its peak, and this is where the oxidation zone ends and the reduction zone starts. This time the CO will be produced by the reduction of CO_2, as this reacts with the char in the bed, consequently reducing the CO_2 and increasing CO concentration as the bed level rises.

Having two measurements instead of one in each axial location of the bed allowed a more definitive observation to be made: the bed presents significant scatter in the gas concentrations, and this is due to random variations in local conditions in the bed, caused by relatively large particles which make the bed not to be a continuous medium, so that the orientation of the particles with respect to the probe, as well as how close they are to it, causes these variations.

The results of volume concentration profiles for three different void fraction models for each particle type are plotted. From their curves it can be said that lowering the void fraction (comparing the average from image analysis and that of unburnt particles) increases the final production of CO while decreasing that of CO_2. The difference becomes bigger if the difference between the void fractions increases (particle type 7 - Figure 5.12 - has the largest difference). The oxidation zone for the lower void fraction becomes thinner, and in this zone the effect of the void fraction is more significant than it is in the rest of the bed. This is evidenced by nearly parallel curves of CO and CO_2 for the void fraction averaged from image analysis and that of unburnt fuel. This behaviour is expected, since the oxidation zone is entirely diffusion controlled ("Regime III" in the designations usually used in the char combustion literature): this regime has a fast oxidation reaction and temperatures are high, so that reaction does not occur inside the particle pores. In this zone, a decrease in void fraction causes an increase in fluid flow velocities as well as an increase

in the specific surface area, which increase the oxidation rate by increasing the mass transfer coefficient which is responsible for transfer of oxygen to the surface. As one moves farther up from this area, the void fraction will play a much smaller role due to a slower reduction reaction, lower temperatures and a partially kinetically controlled region, which gas velocity would not affect as much. The difference between the averaged void fraction model and the empirical linear model also appears consistent with the above-mentioned reasoning, since the void fraction is smallest at the grate surface and increases through the length of the bed for the empirical model. The difference in the final levels of CO and CO_2, and in the thickness of the oxidation zone, is directly related to the void fraction at the grate's surface and that averaged from image analysis.

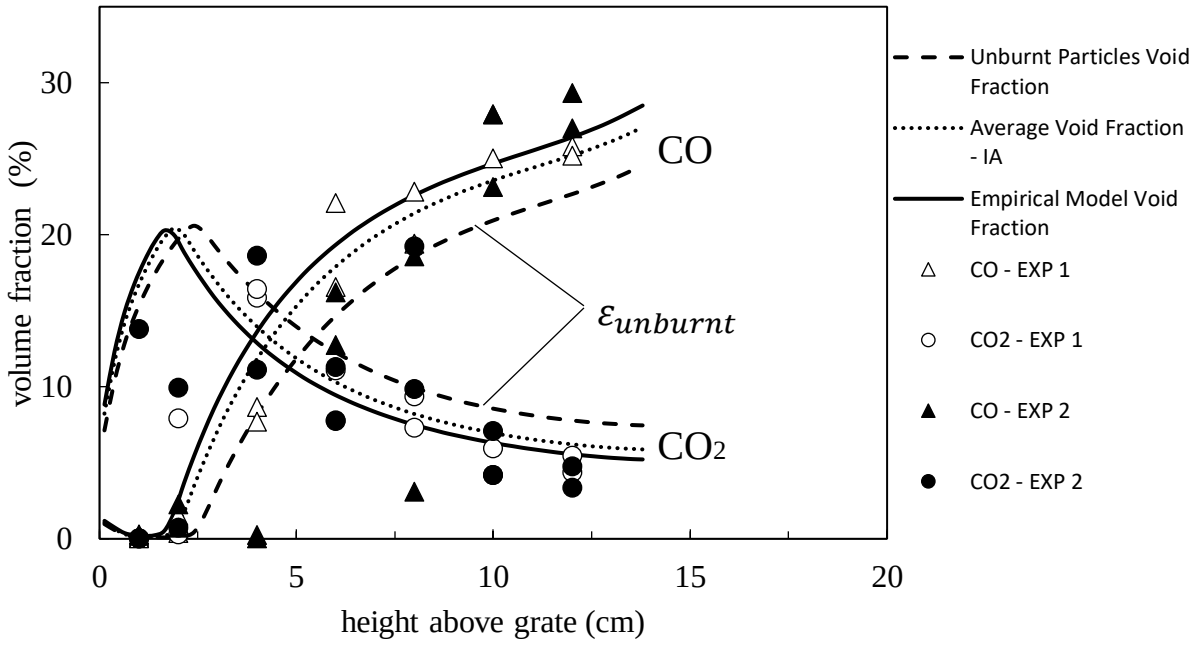

Figure 5.10. Measured (points) and predicted (lines) gas concentrations as functions of height above bed grate for particle type 1. Solid lines, dashed and dotted lines: prediction for trial 1.

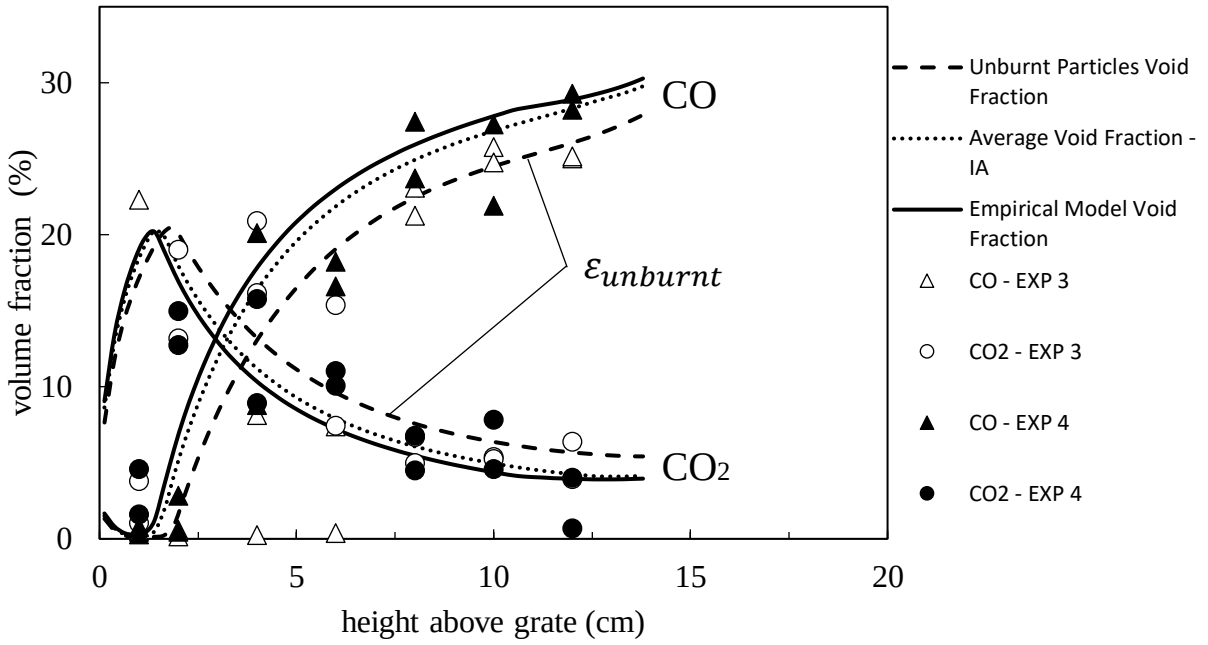

Figure 5.11. Measured (points) and predicted (lines) gas concentrations as functions of height above bed grate for particle type 4. Solid lines, dashed and dotted lines: prediction for trial 3.

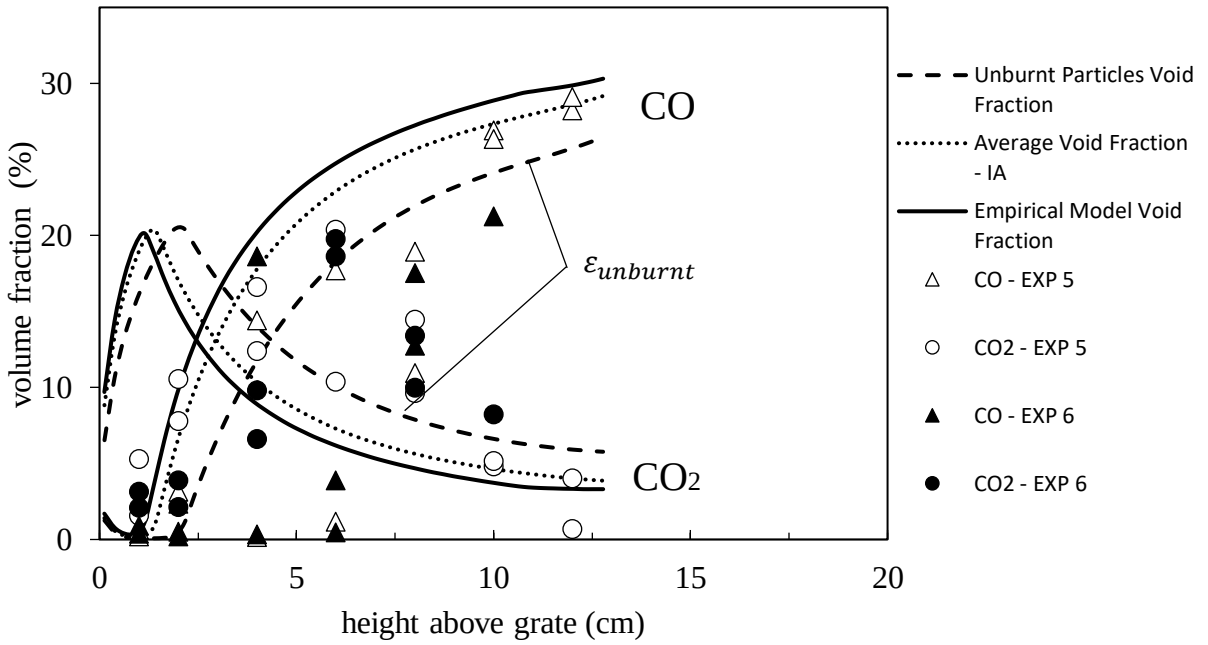

Figure 5.12. Measured (points) and predicted (lines) gas concentrations as functions of height above bed grate for particle type 7. Solid lines, dashed and dotted lines: prediction for trial 5.

Figure 5.13 to Figure 5.15 present the temperatures as a function of height above the grate in the bed, excluding the pyrolysis zone. The thermocouples are located at 1.8, 3.5 and 4.8 cm and their measurements are compared with the model results. As explained previously, the first zone in the bed is the oxidation zone, which is the hottest zone in the bed and it ends roughly at the peak in gas temperature. From this peak onwards, the bed goes though the reduction zone where the gas temperatures have fall gradually towards the top.

The predicted gradients of solid temperatures are much slighter compared to those of the gas. As observed in the graphs of Figure 5.10 to Figure 5.12, the reaction rates near the grate greatly increase as the void fraction decreases, and as a result, the temperature graphs show the effects of this: the temperature peaks are moved closer to the grate as void fraction decreases. Another notable detail is the decrease in the gas temperature peak with decrease of void fraction. The reason for this is that the oxidation zone becomes thinner, and the heat release in this zone will is removed more rapidly by heat losses by conduction and radiation. On the other hand, the solid peak temperature tends to slightly increase, due to an increasing heat transfer from the gases to the solids, given the higher specific surface area of the char and higher transfer coefficients. Again, here the biggest void fraction difference gives rise to a proportionally larger decrease in the gas temperature peak and a larger move of the oxidation zone closer to the bed grate.

Volume fractions, and gas and solid temperatures from the model for averaged void fraction from image analysis and linear void fraction variation agree well with the experimental results. Temperature measurements are more likely to be closer to solid temperatures, owing to the intensity of radiation from the solid.

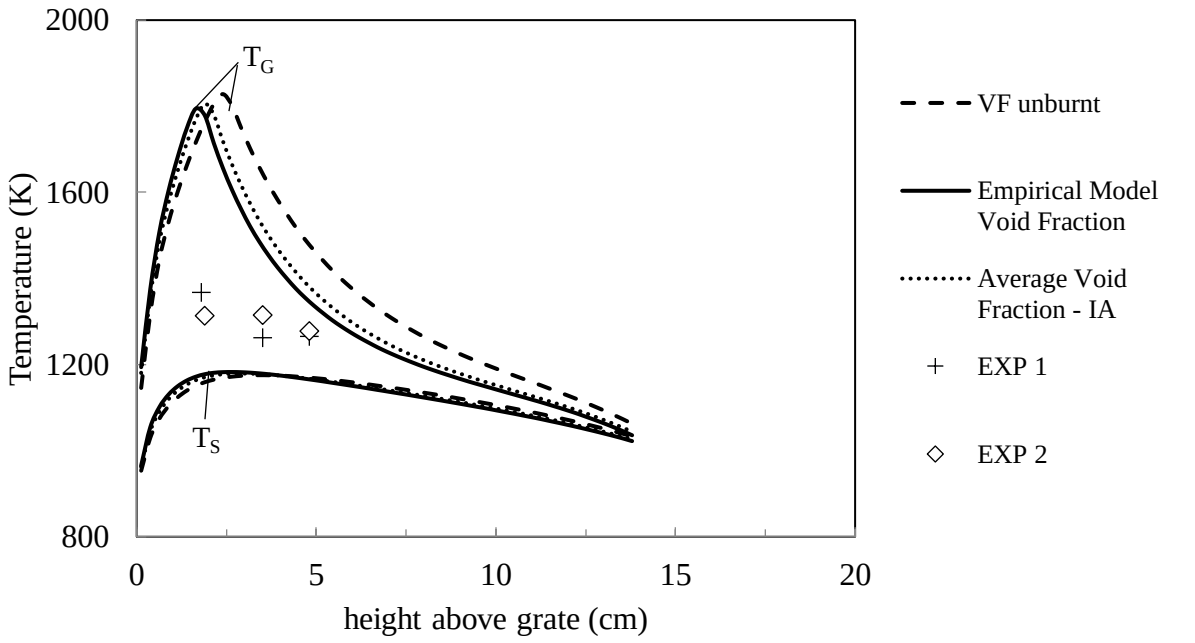

Figure 5.13. Measured (points) and predicted gas (T_G) and solid (T_S) temperatures (lines) as function of height above the grate for particle 1. Measured points are time e average over a 20 minutes window centred around gas analysis time for that particular thermocouple location.

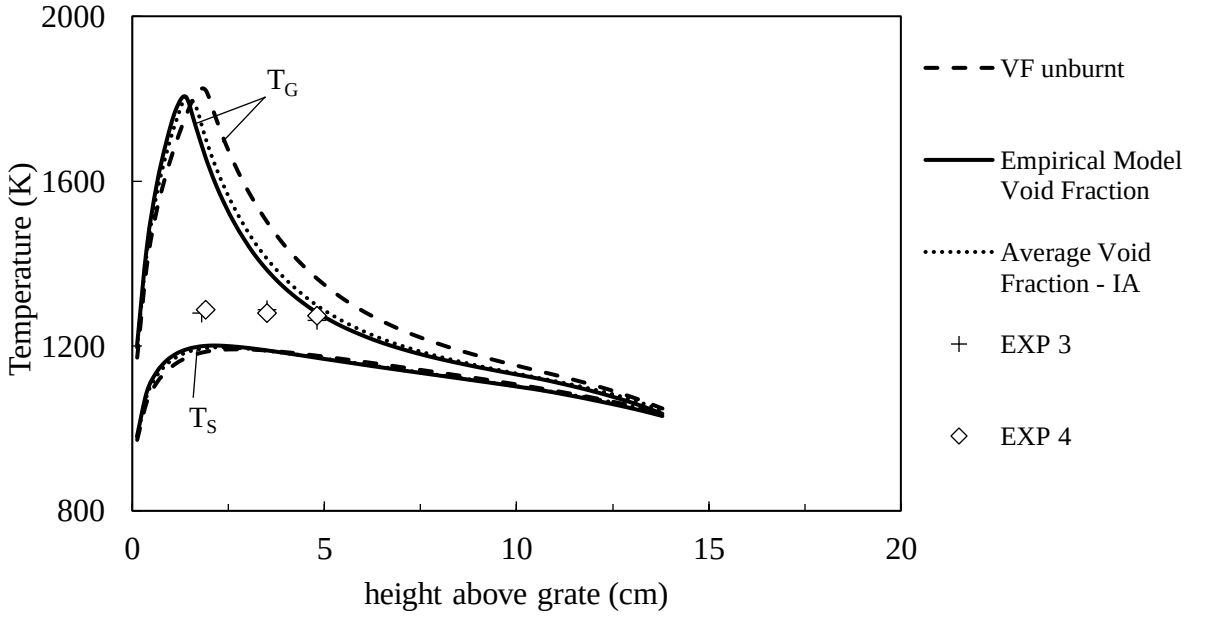

Figure 5.14. Measured (points) and predicted gas (T_G) and solid (T_S) temperatures (lines) as function of height above the grate for particle 4. Measured points are time e average over a 20 minutes window centred around gas analysis time for that particular thermocouple location.

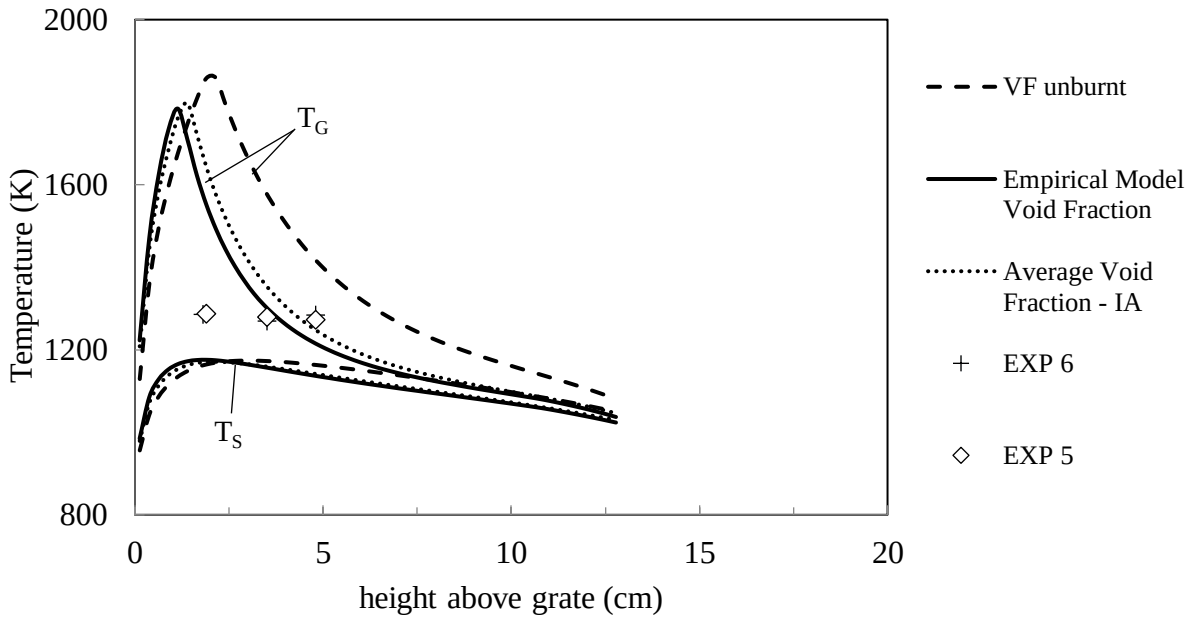

Figure 5.15. Measured (points) and predicted gas (T_G) and solid (T_S) temperatures (lines) as function of height above the grate for particle 7. Measured points are time e average over a 20 minutes window centred around gas analysis time for that particular thermocouple location.

Chapter Six: Conclusions and Recommendations

6.1 Conclusions

In this work the void fraction in a packed bed combustor was investigated with several combustion experiments followed by sampling of the bed. Local void fractions at different heights above the bed grate were found, from which either a linear fitted model for the variation of void fraction with height above the grate or an average of these data could be inserted into an existing 1-D combustion model for comparison with measured temperatures and gas concentrations. These results were compared with those obtained using the assumption that void fraction throughout the bed height is constant and equal to that of unburnt fuel.

Understanding the void fraction in a packed bed combustor has proved of significant importance to the combustion process. The packed bed combustor's local void fractions were measured after each combustion trial by means of solidifying the bed, cutting, and then applying image analysis to the cross sections to binarize the image and then estimate local void fraction at multiple heights above bed grate. The void fraction of a bed of unburnt particles had recently been used to characterize the void fraction of a packed bed combustor, but our experimental results indicate that this assumption tends to overestimate the actual void fraction in a burning bed. This discovery - that the void fraction in the bed of burning particles – is less than that of a bed of unburnt fuel particles – is the most surprising conclusion of this work. It affects local combustion conditions by increasing gas velocities, heat and mass transfer coefficients, and burning rates.

Three different ways of modelling void fraction in the bed have been tried out: an empirical linear model of varying void fraction fitted from the measured variation of void with the length of the bed, a constant bulk void fraction equal to the average of the local measurements, and the well-known method of assuming a constant void fraction equal to that of unburnt fuel particles. The empirical model was developed for the void fraction axial profile: a linear equation varying from lower void fraction at the bottom to higher at the top of the bed. The void fraction results showed how challenging developing a mathematical model can be, given the large scatter of the data, caused by the wide range of stochastic variation in bed structure from point to point. For this reason, assuming a constant (average) void fraction throughout the bed length is still a viable option as

well. Regarding the radial profile of void fraction, a more uniform distribution was found, although having a considerable standard deviation, and this would suggest that the wall effect is not tremendously strong.

The gas volume and temperatures results of the combustion model simulation showed a good agreement with the measurements in the bed, by using both the empirical void fraction model and the constant averaged one. Lowering the void fraction of the bed caused a decrease in the thickness of the oxidation zone in the bed, consequently a thicker reduction zone that allowed more CO production against less CO_2. The peak temperature of the gas was also lowered with a smaller void fraction. By comparing these model simulation results, one can see that the effect of a change of void fraction in the oxidation zone is amplified, giving higher velocities for a diffusion-controlled zone.

Exploring the resulting slabs that gives the cross sections was also an important feature of the method of bed solidification, as it can provide samples of particles at exact different positions in the bed so proximate analysis can be performed.

6.2 Recommendations

Although the void fraction in the bed was found to be lower than previously assumed, and lower than that of a bed of the unburned particles, proving what causes this is still uncertain. One could think of rounding and shrinkage of the particles due to combustion as one moves closer to the grate, but previous works found that the shape of the particle, represented by the sphericity and the particle size, does not vary much in most of the bed, as the only significant variation occurs at the very bottom. Tamping on the bed to avoid bridging and channelling during the experiment could be another explanation; however, this is done slightly so it is likely not responsible for densifying the bed.

Using epoxy resin to fill the voids instead of wax, although much more expensive, could perhaps facilitate the whole local void fraction analysis process and consequently bring information on more regions of the bed, mainly in the most affected diffusion-controlled zone, closer to the grate. The epoxy resin could result in more reading of local void fractions in the bed, by machining the cross sections in smaller intervals. Machining the bed filled with wax isn't recommended given the danger of instantly liquefying the wax with the high speeds. Finally, other features of the bed structure could also be visualized, such as particle overlap, with the use of a transparent resin.

Another possible approach would be to find a means to sample the bed, preserving its structure as has been done here, but without embedding it in wax or resin. Visual methods could then be used to estimate particle overlap, as was done for the unburnt fuel. The challenge would be finding a way to measure void fraction variations.

References

Afandizadeh, S., & Foumeny, E. A. (2001). Design of packed bed reactors: guides to catalyst shape, size, and loading selection. *Applied Thermal Engineering*, *21*(6), 669–682. https://doi.org/10.1016/S1359-4311(00)00072-7

Auwerda, G. J., Kloosterman, J. L., Winkelman, A. J. M., Groen, J., & Van Dijk, V. (2010). Comparison of experiments and calculations of void fraction distributions in randomly stacked pebble beds. PHYSOR 2010-Advances in Reactor Physics to Power the Nuclear Renaissance, 1897-1909.

Bauer, R., Gölles, M., Brunner, T., Dourdoumas, N., & Obernberger, I. (2010). Modelling of grate combustion in a medium scale biomass furnace for control purposes. *Biomass and Bioenergy*, *34*(4), 417–427. https://doi.org/10.1016/j.biombioe.2009.12.005

Beavers, G. S., Sparrow, E. M., & Rodenz, D. E. (1973). Influence of Bed Size on the Flow Characteristics and Porosity of Randomly Packed Beds of Spheres. *Journal of Applied Mechanics*, *40*(3), 655–660. https://doi.org/10.1115/1.3423067

Benenati, R. F., & Brosilow, C. B. (1962). Void fraction distribution in beds of spheres. *AIChE Journal*, *8*(3), 359–361. https://doi.org/10.1002/aic.690080319

Benyahia, F. (1996). On the global and local structural properties of packed beds of nonequilateral cylindrical particles. *Particulate Science and Technology*, *14*(3), 221–237. https://doi.org/10.1080/02726359608906697

Benyahia, F., & O'Neill, K. E. (2007). Enhanced Voidage Correlations for Packed Beds of Various Particle Shapes and Sizes. *Http://Dx.Doi.Org/10.1080/02726350590922242*, *23*(2), 169–177. https://doi.org/10.1080/02726350590922242

Bernal, J. D., & Finney, J. L. (1967). Random Packing of Spheres in Non-rigid Containers. *Nature 1967 214:5085*, *214*(5085), 265–266. https://doi.org/10.1038/214265a0

Berryman, J. G. (1983). Random close packing of hard spheres and disks. *Physical Review A*, *27*(2), 1053. https://doi.org/10.1103/PhysRevA.27.1053

Bunt, J. R., & Waanders, F. B. (2008). An understanding of lump coal physical property behaviour (density and particle size effects) impacting on a commercial-scale Sasol-Lurgi FBDB gasifier. *Fuel*, *87*(13–14), 2856–2865. https://doi.org/10.1016/j.fuel.2008.03.022

Caulkin, R., Ahmad, A., Fairweather, M., Jia, X., & Williams, R. A. (2009). Digital predictions of

complex cylinder packed columns. *Computers & Chemical Engineering*, *33*(1), 10–21. https://doi.org/10.1016/j.compchemeng.2008.06.001

Chen, J. S., & Gunkel, W. W. (1987). Modeling and simulation of co-current moving bed gasification reactors — Part II. A detailed gasifier model. *Biomass*, *14*(2), 75–98. https://doi.org/10.1016/0144-4565(87)90012-6

Comiti, J., & Renaud, M. (1989). A new model for determining mean structure parameters of fixed beds from pressure drop measurements: application to beds packed with parallelepipedal particles. *Chemical Engineering Science*, *44*(7), 1539–1545. https://doi.org/10.1016/0009-2509(89)80031-4

Conradie, F. H., Bunt, J. R., Neomagus, H. W. J. P., Waanders, F. B., & Everson, R. C. (2015). A laboratory scale fixed-bed coal conversion reactor part 1: Operation, reaction zone identification and industrial representativeness. *Journal of Analytical and Applied Pyrolysis*, *115*, 428–436. https://doi.org/10.1016/j.jaap.2015.06.016

Conradie, F. H., Bunt, J. R., & Waanders, F. B. (2016). Coal particle and bed physical transformational behaviour after thermochemical conversion in a fixed bed. *Journal of Analytical and Applied Pyrolysis*, *122*, 45–54. https://doi.org/10.1016/j.jaap.2016.10.024

Cooke, A. J., & Rowe, R. K. (1999). Extension Of Porosity And Surface Area Models For Uniform Porous Media. *Journal Of Environmental Engineering*.

Cooper, A. R., & Eaton, L. E. (1962). Compaction Behavior of Several Ceramic Powders. *Journal of the American Ceramic Society*, *45*(3), 97–101. https://doi.org/10.1111/j.1151-2916.1962.tb11092.x

Cooper, J., & Hallett, W. L. H. (2000). A numerical model for packed-bed combustion of char particles. *Chemical Engineering Science*, *55*(20), 4451–4460. https://doi.org/10.1016/s0009-2509(00)00097-x

Crawford, C. W., & Plumb, O. A. (1986). The Influence of Surface Roughness on Resistance to Flow Through Packed Beds. *Journal of Fluids Engineering*, *108*(3), 343–347. https://doi.org/10.1115/1.3242584

Debbas, S., & Rumpf, H. (1966). On the randomness of beds packed with spheres or irregular shaped particles. *Chemical Engineering Science*, *21*(6–7), 583–608. https://doi.org/10.1016/0009-2509(66)85072-8

Desmond, K. W., & Weeks, E. R. (2009). Random close packing of disks and spheres in confined

geometries. *Physical Review E*, *80*(5), 051305. https://doi.org/10.1103/PhysRevE.80.051305

Dixon, A. G. (1988). Correlations for wall and particle shape effects on fixed bed bulk voidage. *The Canadian Journal of Chemical Engineering*, *66*(5), 705–708. https://doi.org/10.1002/cjce.5450660501

Dorn, M., Eschbach, F., Hekmat, D., & Weuster-Botz, D. (2017). Influence of different packing methods on the hydrodynamic stability of chromatography columns. *Journal of Chromatography A*, *1516*, 89–101. https://doi.org/10.1016/j.chroma.2017.08.019

Duffy, N. T. M., & Eaton, J. A. (2013). Investigation of factors affecting channelling in fixed-bed solid fuel combustion using CFD. *Combustion and Flame*, *160*(10), 2204–2220. https://doi.org/10.1016/j.combustflame.2013.04.015

Ergun, S., & Orning, A. A. (1949). Fluid Flow through Randomly Packed Columns and Fluidized Beds. *Industrial & Engineering Chemistry*, *41*(6), 1179–1184. https://doi.org/10.1021/IE50474A011

Farsi, A., Xiang, J., Latham, J. P., Carlsson, M., Stitt, H., & Marigo, M. (2021). Packing simulations of complex-shaped rigid particles using FDEM: An application to catalyst pellets. *Powder Technology*, *380*, 443–461. https://doi.org/10.1016/j.powtec.2020.11.010

Foumeny, E. A., Moallemi, H. A., Mcgreavy, C., & Castro, J. A. A. (1991). Elucidation of mean voidage in packed beds. *The Canadian Journal of Chemical Engineering*, *69*(4), 1010–1015. https://doi.org/10.1002/cjce.5450690425

Gan, J. Q., Yu, A. B., & Zhou, Z. Y. (2016). DEM simulation on the packing of fine ellipsoids. *Chemical Engineering Science*, *156*, 64–76. https://doi.org/10.1016/j.ces.2016.09.017

Gan, M., Gopinathan, N., Jia, X., & Williams, R. A. (2004). Predicting Packing Characteristics of Particles of Arbitrary Shapes. *KONA Powder and Particle Journal*, *22*(March), 82–93. https://doi.org/10.14356/kona.2004012

Girgis, E., & Hallett, W. L. H. (2010). Wood Combustion in an Overfeed Packed Bed, Including Detailed Measurements within the Bed. *Energy and Fuels*, *24*(3), 1584–1591. https://doi.org/10.1021/ef901206d

Goodling, J. S., Vachon, R. I., Stelpflug, W. S., Ying, S. J., & Khader, M. S. (1983). Radial porosity distribution in cylindrical beds packed with spheres. *Powder Technology*, *35*(1), 23–29. https://doi.org/10.1016/0032-5910(83)85022-0

Gunarathne, D. S., Chmielewski, J. K., & Yang, W. (2014). Pressure drop prediction of a gasifier

bed with cylindrical biomass pellets. *Applied Energy*, *113*, 258–266. https://doi.org/10.1016/j.apenergy.2013.07.032

H Susskind, W. B. (1966). Random packing of spheres in non-rigid containers [8]. *Nature*, *212*(5070), 1564. https://doi.org/10.1038/2121564a0

Hallett, W. (2009). Combustion in Diffusion Systems [Class Handout]. University of Ottawa, MCG 5192.

Hallett, W., Green, B., Machula, T., & Yang, Y. (2013). Packed bed combustion of non-uniformly sized char particles. *Chemical Engineering Science*, *96*, 1–9. https://doi.org/10.1016/j.ces.2013.02.070

Hallett, W. L. H., Busigin, M. K., Berdusco, D., & Wiens, E. (2019). Pressure loss in packed beds of binary mixtures of angular parallelepipeds. *Chemical Engineering Science*, *195*, 578–584. https://doi.org/10.1016/j.ces.2018.09.056

Hamel, S., & Krumm, W. (2008). Near-wall porosity characteristics of fixed beds packed with wood chips. *Powder Technology*, *188*(1), 55–63. https://doi.org/10.1016/j.powtec.2008.03.011

Hamel, S., & Krumm, W. (2012). Radial voidage variation in fixed beds of fuel wood pellets. *Biomass and Bioenergy*, *46*, 203–209. https://doi.org/10.1016/j.biombioe.2012.08.025

Haughey, D. P., & Beveridge, G. S. G. (1969). Structural properties of packed beds — A review. *The Canadian Journal of Chemical Engineering*, *47*(2), 130–140. https://doi.org/10.1002/cjce.5450470206

Hobbs, M. L., Radulovic, P. T., & Smoot, L. D. (1992). Modeling fixed-bed coal gasifiers. *AIChE Journal*, *38*(5), 681–702. https://doi.org/10.1002/aic.690380506

Hoffmann, A. C., & Finkers, H. J. (1995). A relation for the void fraction of randomly packed particle beds. *Powder Technology*, *82*(2), 197–203. https://doi.org/10.1016/0032-5910(94)02910-g

ImageJ. (n.d.). Retrieved November 29, 2021, from https://imagej.nih.gov/ij/

Jia, X., Gan, M., Williams, R. A., & Rhodes, D. (2007). Validation of a digital packing algorithm in predicting powder packing densities. *Powder Technology*, *174*(1–2), 10–13. https://doi.org/10.1016/j.powtec.2006.10.013

Klerk, A. de. (2003). Voidage variation in packed beds at small column to particle diameter ratio. *AIChE Journal*, *49*(8), 2022–2029. https://doi.org/10.1002/aic.690490812

Koekemoer, A., & Luckos, A. (2015). Effect of material type and particle size distribution on pressure drop in packed beds of large particles: Extending the Ergun equation. *Fuel*, *158*, 232–238. https://doi.org/10.1016/j.fuel.2015.05.036

Krishnudu, T., Madhusudhan, B., Reddy, S. N., Sastry, V. S. R., Vaidyeswaran, R., & Rao, K. S. (1989). Studies in a Moving Bed Pressure Gasifier: Prediction of Reaction Zones and Temperature Profile. *Industrial and Engineering Chemistry Research*, *28*(4), 438–444. https://doi.org/10.1021/ie00088a011

Küfner, R., & Hofmann, H. (1990). Implementation of radial porosity and velocity distribution in a reactor model for heterogeneous catalytic gasphase reactions (TORUS-Model). *Chemical Engineering Science*, *45*(8), 2141–2146. https://doi.org/10.1016/0009-2509(90)80088-V

Lee, Q. F., & Bennington, C. P. J. (2005). The Effect of Particle Size Distribution on Pressure Drop through Packed Beds of Cooked Wood Chips. *The Canadian Journal of Chemical Engineering*, *83*(4), 755–763. https://doi.org/10.1002/cjce.5450830416

Luckos, A., & Bunt, J. R. (2011). Pressure-drop predictions in a fixed-bed coal gasifier. *Fuel*, *90*(3), 917–921. https://doi.org/10.1016/j.fuel.2010.09.020

Lufeng Liu, Zhuoran Li, Yang Jiao, & Shuixiang Li. (2017). Maximally dense random packings of cubes and cuboids via a novel inverse packing method. *Soft Matter*, *13*(4), 748–757. https://doi.org/10.1039/c6sm02065h

Macrae, J. C., & Gray, W. A. (1961). Significance of the properties of materials in the packing of real spherical particles. *British Journal of Applied Physics*, *12*(4), 164. https://doi.org/10.1088/0508-3443/12/4/309

Man, W., Donev, A., Stillinger, F. H., Sullivan, M. T., Russel, W. B., Heeger, D., Inati, S., Torquato, S., & Chaikin, P. M. (2005). Experiments on Random Packings of Ellipsoids. *Physical Review Letters*, *94*(19), 198001. https://doi.org/10.1103/PhysRevLett.94.198001

Mangena, S. J., Bunt, J. R., & Waanders, F. B. (2013). Physical property behaviour of North Dakota lignite in an oxygen/steam blown moving bed gasifier. *Fuel Processing Technology*, *106*, 326–331. https://doi.org/10.1016/j.fuproc.2012.08.016

McGEARY, R. K. (1961). Mechanical Packing of Spherical Particles. *Journal of the American Ceramic Society*, *44*(10), 513–522. https://doi.org/10.1111/J.1151-2916.1961.tb13716.x

Mehrabian, R., Shiehnejadhesar, A., Scharler, R., & Obernberger, I. (2014). Multi-physics modelling of packed bed biomass combustion. *Fuel*, *122*(2014), 164–178.

https://doi.org/10.1016/j.fuel.2014.01.027

Milewski, J. V. (1973). *A Study of the Packing of Fibers and Spheres*. Rutgers University.

Montillet, A., & Coq, L. Le. (2003). Image Analysis: A Useful Tool for Porous Media Characterization. *Chemical Engineering & Technology*, *26*(12), 1285–1289. https://doi.org/10.1002/CEAT.200310020

Montillet, A., & Le Coq, L. (2001). Characteristics of fixed beds packed with anisotropic particles - Use of image analysis. *Powder Technology*, *121*(2–3), 138–148. https://doi.org/10.1016/S0032-5910(01)00332-1

Nguyen, N. L., Van Buren, V., Reimert, R., & Von Garnier, A. (2005). Determination of porosity and flow distribution in packed beds by magnetic resonance imaging. *Magnetic Resonance Imaging*, *23*(2 SPEC. ISS.), 395–396. https://doi.org/10.1016/j.mri.2004.11.061

Niu, M., Akiyama, T., Takahashi, R., & Yagi, J. (1996). Reduction of the wall effect in a packed bed by a hemispherical lining. *AIChE Journal*, *42*(4), 1181–1186. https://doi.org/10.1002/AIC.690420432

Nolan, G. T., & Kavanagh, P. E. (1995). Random packing of nonspherical particles. *Powder Technology*, *84*(3), 199–205. https://doi.org/10.1016/0032-5910(95)98237-S

Ozawa, M., Umekawa, H., Matsuda, T., Takenaka, N., Tsuruno, A., & Matsubayashi, M. (1996). Void fraction profile in tube-banks of a simulated fluidized-bed heat exchanger. *Nuclear Instruments and Methods in Physics Research Section A: Accelerators, Spectrometers, Detectors and Associated Equipment*, *377*(1), 144–147. https://doi.org/10.1016/0168-9002(96)00131-3

Pillai, K. K. (1977). Voidage variation at the wall of a packed bed of spheres. *Chemical Engineering Science*, *32*(1), 59–61. https://doi.org/10.1016/0009-2509(77)80195-4

Porteiro, J., Patiño, D., Collazo, J., Granada, E., Moran, J., & Miguez, J. L. (2010). Experimental analysis of the ignition front propagation of several biomass fuels in a fixed-bed combustor. *Fuel*, *89*(1), 26–35. https://doi.org/10.1016/j.fuel.2009.01.024

Pottbäcker, J., & Hinrichsen, O. (2017). Experimental Study on the Influence of Filling Method and Particle Material on the Packed-Bed Porosity. *Chemie Ingenieur Technik*, *89*(4), 454–458. https://doi.org/10.1002/cite.201600151

R. Farrell, G., Michael Martini, K., & Narayanan Menon. (2010). Loose packings of frictional spheres. *Soft Matter*, *6*(13), 2925–2930. https://doi.org/10.1039/c0sm00038h

Raichura, R. C. (2010). Pressure Drop And Heat Transfer In Packed Beds With Small Tube-To-Particle Diameter Ratio. *Http://Dx.Doi.Org/10.1080/089161599269627*, *12*(4), 309–327. https://doi.org/10.1080/089161599269627

Rbunt, J. (2006). *a New Dissection Methodology and Investigation Into Coal Property Transformational Behaviour Impacting on a Commercial-Scale Sasol-Lurgi Mk Iv Fixed-Bed Gasifier*. *May*.

Ridgway, K., & Tarbuck, K. J. (1966). Radial voidage variation in randomly-packed beds of spheres of different sizes. *Journal of Pharmacy and Pharmacology*, *18*(S1), 168S-175S. https://doi.org/10.1111/J.2042-7158.1966.tb07980.x

Roblee, L. H. S., Baird, R. M., & Tierney, J. W. (1958). Radial porosity variations in packed beds. *AIChE Journal*, *4*(4), 460–464. https://doi.org/10.1002/aic.690040415

Romanova, T., Litvinchev, I., & Pankratov, A. (2020). Packing ellipsoids in an optimized cylinder. *European Journal of Operational Research*, *285*(2), 429–443. https://doi.org/10.1016/j.ejor.2020.01.051

Ryan, J. S., & Hallett, W. L. H. (2002). Packed bed combustion of char particles: Experiments and an ash model. *Chemical Engineering Science*, *57*(18), 3873–3882. https://doi.org/10.1016/S0009-2509(02)00235-x

Ryu, C., Yang, Y. Bin, Khor, A., Yates, N. E., Sharifi, V. N., & Swithenbank, J. (2006). Effect of fuel properties on biomass combustion: Part I. Experiments - Fuel type, equivalence ratio and particle size. *Fuel*, *85*(7–8), 1039–1046. https://doi.org/10.1016/j.fuel.2005.09.019

Schneider, F. A., & Rippin, D. W. T. (1988). Determination of the Local Voidage Distribution in Random Packed Beds of Complex Geometry. *Industrial and Engineering Chemistry Research*, *27*(10), 1936–1941. https://doi.org/10.1021/ie00082a030

Schuster, J., & Vortmeyer, D. (1980). Ein einfaches Verfahren zur näherungsweisen Bestimmung der Porosität in Schüttungen als Funktion des Wandabstandes. *Chemie Ingenieur Technik*, *52*(10), 848–849. https://doi.org/10.1002/cite.330521023

Sharma, S., Mantle, M. D., Gladden, L. F., & Winterbottom, J. M. (2001). Determination of bed voidage using water substitution and 3D magnetic resonance imaging, bed density and pressure drop in packed-bed reactors. *Chemical Engineering Science*, *56*(2), 587–595. https://doi.org/10.1016/S0009-2509(00)00264-5

Singh, H., Saini, R. P., & Saini, J. S. (2010). A review on packed bed solar energy storage systems.

Renewable and Sustainable Energy Reviews, *14*(3), 1059–1069. https://doi.org/10.1016/j.rser.2009.10.022

Sohn, H. Y., & Moreland, C. (1968). The effect of particle size distribution on packing density. *The Canadian Journal of Chemical Engineering*, *46*(3), 162–167. https://doi.org/10.1002/CJCE.5450460305

Taguchi, I., Kurashige, M., & Imai, K. (2006). Effects of Cubic Container's Wall or Floor on Random Packing Structures of Spherical Particles. *JSME International Journal Series A Solid Mechanics and Material Engineering*, *49*(2), 265–272. https://doi.org/10.1299/JSMEA.49.265

Tangri, H., Guo, Y., & Curtis, J. S. (2017). Packing of cylindrical particles: DEM simulations and experimental measurements. *Powder Technology*, *317*, 72–82. https://doi.org/10.1016/J.POWTEC.2017.03.058

Thunman, H., & Leckner, B. (2005). Influence of size and density of fuel on combustion in a packed bed. *Proceedings of the Combustion Institute*, *30*(2), 2939–2946. https://doi.org/10.1016/J.PROCI.2004.07.010

Trudel, É., & Hallett, W. (2017). Pressure drop in packed beds of angular parallelepipeds, including the effects of particle interference. *Chemical Engineering Science*, *162*, 209–217. https://doi.org/10.1016/J.CES.2017.01.004

Trudel, É., Hallett, W. L. H., Wiens, E., O'Neil, J. D., Busigin, M. K., & Berdusco, D. (2018). Fuel particle shape effects in the packed bed combustion of wood. *Combustion and Flame*, *198*, 100–111. https://doi.org/10.1016/j.combustflame.2018.09.006

Van Der Lans, R. P., Pedersen, L. T., Jensen, A., Glarborg, P., & Dam-Johansen, K. (2000). Modelling and experiments of straw combustion in a grate furnace. *Biomass and Bioenergy*, *19*(3), 199–208. https://doi.org/10.1016/S0961-9534(00)00033-7

von Seckendorff, J., & Hinrichsen, O. (2020). Review on the structure of random packed-beds. *Canadian Journal of Chemical Engineering*, 1–73. https://doi.org/10.1002/cjce.23959

Westman, A. E. R., & Hugill, H. R. (1930). The Packing Of Particles. *Journal of the American Ceramic Society*, *13*(10), 767–779. https://doi.org/10.1111/J.1151-2916.1930.tb16222.x

Yang, Y. Bin, Ryu, C., Khor, A., Yates, N. E., Sharifi, V. N., & Swithenbank, J. (2005). Effect of fuel properties on biomass combustion. Part II. Modelling approach—identification of the controlling factors. *Fuel*, *84*(16), 2116–2130. https://doi.org/10.1016/j.fuel.2005.04.023

Yang, Y. B., Nasserzadeh, V., Goodfellow, J., & Swithenbank, J. (2003). Simulation of Channel Growth in a Burning Bed of Solids. *Chemical Engineering Research and Design*, *81*(2), 221–232. https://doi.org/10.1205/026387603762878683

Yu, A. -B, Standish, N., & McLean, A. (1993). Porosity Calculation of Binary Mixtures of Nonspherical Particles. *Journal of the American Ceramic Society*, *76*(11), 2813–2816. https://doi.org/10.1111/J.1151-2916.1993.tb04021.x

Yu, A. -B, Zou, R. -P, & Standish, N. (1992). Packing of Ternary Mixtures of Nonspherical Particles. *Journal of the American Ceramic Society*, *75*(10), 2765–2772. https://doi.org/10.1111/J.1151-2916.1992.tb05502.x

Yu, A. B., & Standish, N. (1993). Characterisation of non-spherical particles from their packing behaviour. *Powder Technology*, *74*(3), 205–213. https://doi.org/10.1016/0032-5910(93)85029-9

Zhang, C., Gao, J., Xu, Y., Xia, Y., Wei, X., Su, X., & Zeng, L. (2021). Random loose packing of cylindrical particles considering filling rate. *Powder Technology*, *386*, 98–107. https://doi.org/10.1016/j.powtec.2021.03.027

Zobel, N., Eppinger, T., Behrendt, F., & Kraume, M. (2012). Influence of the wall structure on the void fraction distribution in packed beds. *Chemical Engineering Science*, *71*, 212–219. https://doi.org/10.1016/j.ces.2011.12.029

Zou, R. P., & Yu, A. B. (1995). The packing of spheres in a cylindrical container: the thickness effect. *Chemical Engineering Science*, *50*(9), 1504–1507. https://doi.org/10.1016/0009-2509(94)00483-8

Zou, R. P., & Yu, A. B. (1996). Evaluation of the packing characteristics of mono-sized non-spherical particles. *Powder Technology*, *88*(1), 71–79. https://doi.org/10.1016/0032-5910(96)03106-3